Ore Geology Reviews 115 (2019) 103175

Contents lists available at ScienceDirect

Ore Geology Reviews

journal homepage: www.elsevier.com/locate/oregeorev

# Distribution and occurrence of Ge and related trace elements in sphalerite from the Lehong carbonate-hosted Zn-Pb deposit, northeastern Yunnan, China: Insights from SEM and LA-ICP-MS studies

Chen Wei[a,b], Lin Ye[a,*], Yusi Hu[a,b], Leonid Danyushevskiy[c], Zhenli Li[a,b], Zhilong Huang[a]

[a] State Key Laboratory of Ore Deposit Geochemistry, Institute of Geochemistry, Chinese Academy of Sciences, Guiyang 550081, China
[b] University of Chinese Academy of Sciences, Beijing 100049, China
[c] ARC Centre of Excellence in Ore Deposits, University of Tasmania, Private Bag 79, Hobart, TAS, 7001, Australia

ARTICLE INFO

*Keywords:*
Trace elements in sphalerite
LA-ICP-MS mapping
SEM analysis
Germanium
Sichuan-Yunan-Guizhou (S-Y-G) metallogenic province

ABSTRACT

The rapid increase in the economic importance of germanium (Ge) is driving further study of its geological cycle and the factors controlling its concentration in minerals. The emerging LA-ICP-MS analytic technique is playing a significant insight into the geochemical characteristics of sphalerite. In this study, LA-ICP-MS and SEM analyses were carried out, aiming to constrain the substitution mechanisms of Ge and related trace elements and to trace the evolution of hydrothermal fluids.

LA-ICP-MS element mapping and SEM study showed that no Ge-bearing micro-minerals are observed in the Lehong deposit. All spot analysis data indicate notable binary correlations between Cu and Ge and between Ag and Sb, which suggests that the coupled substitutions are $3Zn^{2+} \leftrightarrow 2Cu^{+} + Ge^{4+}$ and $2Zn^{2+} \leftrightarrow Ag^{+} + Sb^{3+}$. Additionally, the monovalent elements, i.e., Cu and Ag, approximately equal to the sum of all trivalent and tetravalent elements; thus, we consider that the monovalent cations may provide the charge-balance in all of the coupled substitutions responsible for incorporating a wide range of trivalent and tetravalent cations, especially In, Sn, Sb, and Ge, in sphalerite at Lehong.

The trace elements in sphalerite from two hydrothermal stages in the Lehong deposit differ significantly. Early red-brown sphalerite is more enriched in Fe, Ge, Cu, Sb and Ag than late yellow-brown sphalerite, suggesting that trace elements in sphalerite may have the potential to record the evolution of hydrothermal fluids. Early sphalerite is rich in Fe and Ge simultaneously, which points toward coupled behavior of Fe and Ge. *In situ* LA-ICP-MS data from sphalerite at Lehong show that the Cu contents in all samples are nearly double those of Ge. Copper enriched in early sphalerite is an essential factor to promote the substitution of Ge, which results in the coupling of Fe and Ge in sphalerite during the evolution of hydrothermal fluids. In addition, sphalerite at depth is more enriched in Mn, Ge, Cu and Cd than shallow sphalerite. There is a clear upward trend among Mn, Ge, Cu and Cd in sphalerite with increasing depth at Lehong. This relationship may be applied for exploration targeting.

## 1. Introduction

The economic importance of germanium (Ge) is rapidly increasing due to its major applications in modern high-tech industries, e.g., electronics, infrared and fiber optics (Thomas et al., 2000; Höll et al., 2007, Cugerone et al., 2018). Thus, it is necessary to understand its geological cycle and the factors that control its concentrations in host minerals. Ge is one of the most dispersed elements in the Earth's crust, averaging approximately 1.3 ppm Ge (Hu and Gao, 2008), and most Ge is largely incorporated with low concentrations in silicate minerals because of the isovalent substitution by $Ge^{4+}$ of the chemically similar $Si^{4+}$ (Bernstein, 1985). Conversely, Ge exhibits siderophile, chalcophile and organophile behaviors; as a result, the enrichment of Ge mainly occurs in iron-nickel meteorites, Zn-rich and/or Cu-rich sulfide ore deposits, coal and lignitized wood (Bernstein, 1985; Pokrovski and Schott, 1998). Currently, Ge is commercially extracted from some Ge-rich lignite and coal and from zinc concentrate from some Zn-Pb deposits, in particular low-temperature hydrothermal systems (e.g., Mississippi Valley-type (MVT) deposits and vein-type Ag-Pb-Zn deposits), in which Ge is mainly hosted within sphalerite (ZnS) (Bernstein, 1985; Höll et al., 2007). For instance, Ge is concentrated in sphalerite from a vein-type Zn-Ge-Ag-(Pb-Cd) deposit in southeastern France in amounts

* Corresponding author.
*E-mail address:* yelin@vip.gyig.ac.cn (L. Ye).

https://doi.org/10.1016/j.oregeorev.2019.103175
Received 30 December 2018; Received in revised form 12 September 2019; Accepted 13 October 2019
Available online 15 October 2019

up to 2600 ppm (Halfon and Rosique, 1973).

Ge occurrence in sphalerite has long been the subject of debate. Johan et al. (1983) and Johan and Oudin (1986) consider that Ge-bearing minerals occur as microscopic inclusions (e.g., argutite, brunogeierite and briartite) in sphalerite from the French Pyrenees. In contrast, some authors favor the incorporation of $Ge^{2+}$ or $Ge^{4+}$ into the sphalerite structure (Cook et al., 2009, 2015; Ye et al., 2011; Belissont et al., 2014; Bonnet et al., 2017). For example, Cook et al. (2015) confirmed the presence of $Ge^{4+}$ and proposed the $2Zn^{2+} \leftrightarrow Ge^{4+} + \square$ (vacancy) substitution for the incorporation of Ge (up to 1000 ppm) in Fe-rich Cu (up to 8.72 wt%) sphalerite from Tres Marias carbonate-hosted Zn-Pb-(Ge) deposit in Mexico due to lack of correlation between Ge and monovalent ions, i.e., Ag and Cu, for charge compensation. Nevertheless, Bonnet et al. (2017) inferred that the intake of $Ge^{2+}$ in sphalerite occurs in the tetrahedral divalent metal site surrounded by sulfide atoms, suggesting that Ge might be directly substituted as $Ge^{2+}$ for $Zn^{2+}$ ($Ge^{2+} \leftrightarrow Zn^{2+}$) in Ge-rich sphalerite from the MVT deposit in the Central and Eastern Tennessee mining district, United States.

Since the geochemical characteristics of sphalerite were first reported by Oftedahl (1940), several remarkable studies have been published. Notably, a wide range of minor/trace elements (e.g., Ga, In, and Cd) can substitute for $Zn^{2+}$ within the sphalerite structure, offering by-products in sphalerite processing (Höll et al., 2007). The close relationship between minor/trace elements (e.g., Mn, Fe, In, Ge and Ga) in sphalerite and its formation temperature has been used to restrict the ore-forming temperature (e.g., Warren et al., 1945; Möller, 1987; Möller and Dulski, 1996, Frenzel et al., 2016 and references therein). Trace elements in sphalerite from different genesis of Zn-Pb deposits have obvious differences, which can to a large extent be used to discriminate the genetic type (e.g., Zhang, 1987; Cook et al., 2009; Ye et al., 2011, 2016; Belissont et al., 2014; Wei et al., 2018a,b). To date, however, information about whether trace elements in sphalerite can be used to trace the evolution process of hydrothermal fluids is still scarce.

To understand the distribution and occurrence of Ge and related trace elements in sphalerite, the Lehong carbonate-hosted Zn-Pb deposit, in the Sichuan-Yunan-Guizhou (S-Y-G) Zn-Pb metallogenic province, Southwest China (Fig. 1), is taken as an example. We present an integrated geological, mineralogical and geochemical study on sphalerite. Ge and related trace elements, including Sb, Ag and Cu, are relatively enriched in sphalerite from the Lehong deposit. Trace element concentrations in sphalerite were measured using LA-ICP-MS spot analysis. SEM and LA-ICP-MS mapping were further used to obtain the occurrence of trace elements in sphalerite.

## 2. Geologic setting

The Yangtze Block is a significant part of the South China Craton and is bounded by the Qinling-Dabie Orogenic Belt to the north, the Songpan-Ganzê Orogenic Belt to the northwest, the North Vietnam tectonic belt to the southwest and the Cathaysia Block to the southeast (Fig. 1A). The exposed strata in the Yangtze Block are dominated by the Mesoproterozoic to early Neoproterozoic basement, the middle Neoproterozoic weakly metamorphosed strata, the late Neoproterozoic unmetamorphosed Ediacaran rocks, and Phanerozoic cover (Yan et al., 2003).

The S-Y-G triangle district is located on the southwestern margin of the Yangtze Block. The basement comprises mainly the Mesoproterozoic to Neoproterozoic Kunyang Group, which consists dominantly of sandstone, siltstone, slate, shale and dolostone with minor volcanic rocks (Li et al., 1984) and has experienced greenschist facies metamorphism. Some authors consider that the Kunyang Group was deposited in a foreland basin setting (e.g., Sun et al., 2009; Li et al., 2013). The overlying cover strata are made up of Neoproterozoic Ediacaran to Middle Triassic shallow submarine carbonate and clastic sedimentary sequences in a passive continental margin. Following the Middle Triassic strata are Late Triassic to Cenozoic continental sedimentary rocks (e.g., Liu and Lin 1999; Yan et al. 2003). One of the significant characteristics of the western Yangtze Block is that a mantle plume erupted and formed the remarkable Emeishan Large Igneous Province (~260 Ma), covering an area of more than 250,000 $km^2$ (e.g., Zhou et al., 2002; He et al., 2007). The igneous province is dominantly composed of massive flood basalts and numerous contemporaneous mafic and felsic intrusions with a total thickness ranging from several hundred meters to 5 km (He et al., 2007). During the Late Triassic, the collision of the Yangtze Block and the adjacent blocks, i.e., Yidun Arc, leading to the closure of the Paleo-Tethys Ocean (e.g., Reid et al., 2007; Zhang et al., 2015).

The faults within the S-Y-G triangle district are well developed and have been activated and reactivated by a number of tectonic events, including the Hercynian, Indosinian, and Yanshanian orogenic events. The three most important regional fault belts (Fig. 1B), namely, the NW-trending Weining–Shuicheng, the N-trending Anninghe, and the NE-trending Mile–Shizong fault belts, extend into basement rocks and control the magmatism and base metal sulfide mineralization (Liu and Lin, 1999). Numerous NE- and NW-trending thrust-fold belts and several subsidiary faults are widespread in this district (e.g., Wang et al., 1992; Huang et al., 2004).

Carbonate-hosted Zn-Pb deposits are widely distributed in the S-Y-G triangular district (Fig. 1B) and have a proven reserves > 200 Mt ores at ore grades of 10–15 wt% Zn + Pb (Zhang et al., 2015). These deposits are epigenetic and hosted in the Ediacaran to Early Permian carbonate strata, particularly the Late Ediacaran Dengying and Early Carboniferous formations (Liu and Lin 1999; Huang et al., 2004; Jin et al., 2008). The major features of these deposits are as follows: (1) most Pb-Zn orebodies are lentiform to vein shaped and controlled by faults; (2) Pb + Zn ore grades are high (10–30 wt%), and ore grades of a few deposits, e.g., Huize and Fule, exceed 50 wt% and are accompanied by Ag, Ge, Cd, Ga, and In (Huang et al., 2004; Han et al., 2007); (3) ore-forming temperatures were typically 150 °C to 270 °C; and (4) ore fluids were basinal brines with 6.0 to 20 wt% NaCl equiv. In addition, recent Rb-Sr dating of sphalerite and Sm-Nd dating of hydrothermal fluorite/calcite indicate that these carbonate-hosted Zn-Pb deposits mainly formed between 226 Ma and 201 Ma (e.g., Li et al., 2007; Lin et al., 2010; Wu, 2013; Zhang et al., 2015; Hu et al., 2017); thus, some researchers suppose that the Indosinian Orogeny triggered regional migration of the basinal brines that leached ore-forming elements from basement rocks to form the world class S-Y-G Zn-Pb metallogenic province (e.g., Zhang et al., 2015; Hu et al., 2017).

## 3. Geology of the Lehong deposit

The Lehong deposit (27°10N, 103°13 E) is located in the northeast part of the S-Y-G region, 26 km northwest of Ludian city, Yunnan Province. It has been mined since the end of the Ming Dynasty and has a proven reserves of 2.4 Mt metal at ore grades of 0.8–30.80 wt% Zn, 0.6–15.57 wt% Pb, and 7.22–148.0 g/t Ag (Zhou, 2003). Over the past two decades, several geological and geochemical studies have been carried out on the Lehong Zn-Pb deposit, most of which were published in Chinese. The genetic model of the Lehong deposit has been extensively reviewed by Zhou (2003), and additional stable isotope studies, geochronology and fluid inclusion studies were carried out by Zhang et al. (2014) and Zhao et al. (2018). Zhang et al. (2014) considered that sulfur was derived from seawater sulfate and that thermochemical sulfate reduction (TSR) was the dominant mechanism for the incorporation of $S^{2-}$ from SO based on the sulfur isotope signatures, and the Rb-Sr dating of sphalerite showed that the Lehong deposit formed at 200.9 ± 8.3 Ma, as a product of the Indosinian orogeny (Zhang et al., 2014). In addition, Zhao et al. (2018) demonstrated that the early stage hydrothermal fluid was characterized by moderate-salinity $H_2O$-$CO_2$-NaCl fluid (7.02–17.61 wt% NaCl equiv.) at 217.8–292.2 °C, and the late stage hydrothermal fluid was

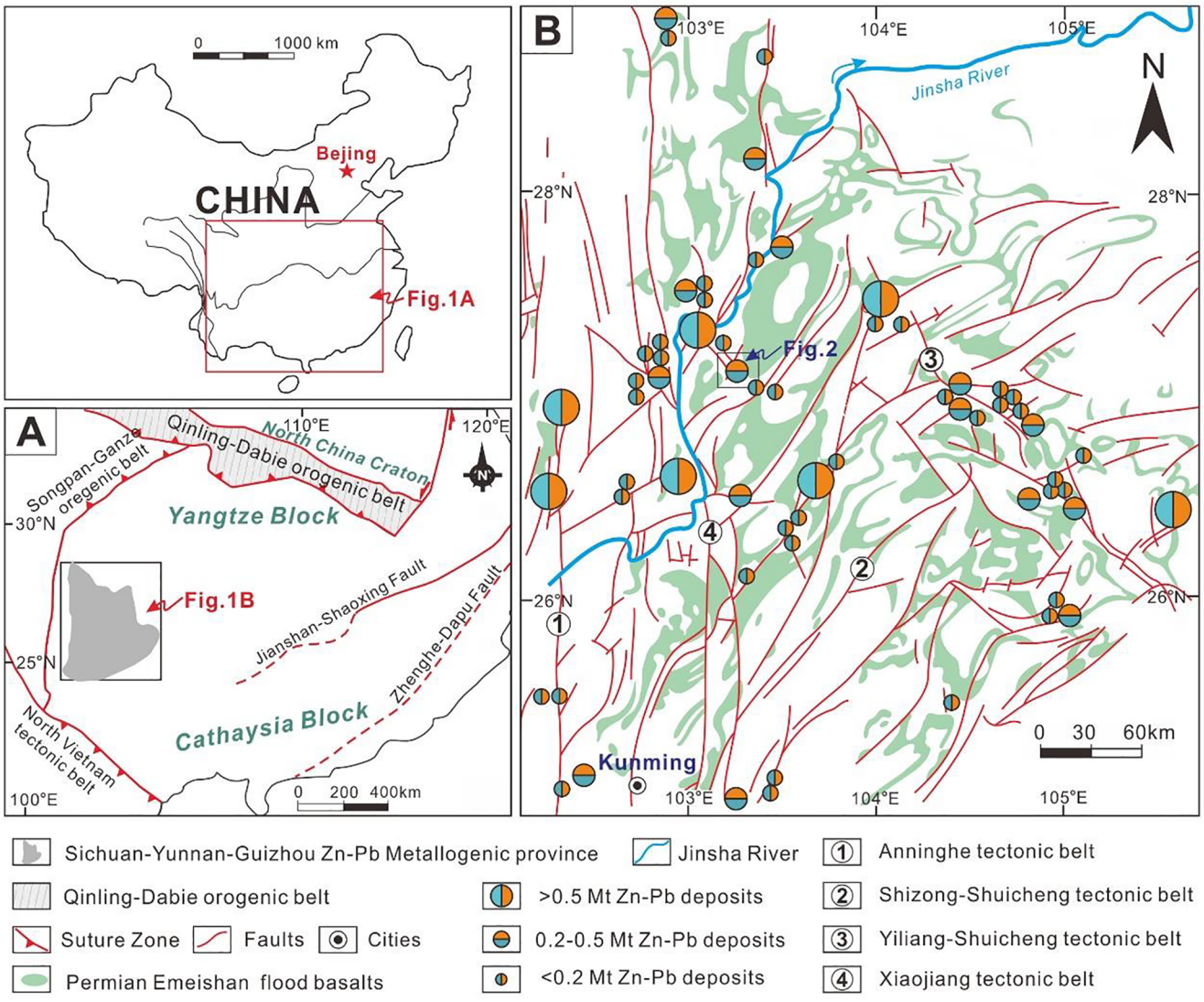


**Fig. 1.** A. The simplified geological map of the South China Craton and adjacent regions showing the framework and the distribution of Mississippi Valley-type (MVT) Zn-Pb deposits in the Yangtze Block (Modified after Ye et al., 2011; Hu et al., 2017). B. The geological map of the Sichuan-Yunnan-Guizhou (S-Y-G) Zn-Pb metallogenic province showing the locations of zinc-lead deposits (Modified after Liu and Lin, 1999).

characterized by low- to moderate-salinity $H_2O$-$CO_2$-NaCl fluid (0.35–19.21 wt% NaCl equiv.) at low temperatures (140.4–227.4 °C).

The exposed strata in the Lehong mining area include Neoproterozoic Ediacaran rocks and early Paleozoic Cambrian and Ordovician rocks (Fig. 2). The late Ediacaran Dengying Formation is composed of light gray thick-bedded coarse-grained dolostone and siliceous dolostone, which is overlain by Cambrian strata that are composed dominantly of dolostone intercalated with siltstone and mudstone. Overlying the Cambrian strata are the Ordovician layers, which consist mainly of mudstone, sandstone and dolostone.

The mining area is characterized by a set of N- to E-W-trending faults, subsidiary faults of the N-trending faults, and minor secondary NE-trending faults (Fig. 2A). The $F_1$, $F_2$ and $F_5$ faults are the most important faults in the mine area. The $F_1$ thrust fault strikes 300–340° with a length of 2000 m and is cut by the $F_5$ fault in the southern part of the mining area (Fig. 2A). The late Ediacaran Dengying Formation is exposed on both sides of the $F_1$ fault. The $F_2$ fault, located in the west part of the orefield, is a thrust fault and strikes 310–340° with a length of 2500 m. Cambrian and Ordovician strata are mainly exposed in the southwest part of the $F_1$ fault. The northeast part of the $F_1$ fault exposes the late Ediacaran Dengying Formation. The $F_5$ fault, a normal fault, strikes approximately 90° with a length of 1000 m, cuts across the $F_4$ and $F_2$ faults and finally merges with the $F_3$ fault.

Three orebodies have been explored in the Lehong mining area, most of which are hosted within the NW-trending $F_1$, $F_2$ and $F_3$ faults (Fig. 2B). They have been divided into orebody I, orebody II and orebody III. Orebody I is the second largest orebody in the Lehong deposit and hosted within the $F_1$ fault (Fig. 2B). Its orebodies occur as lentiform shapes or as veins within the fault fracture zone and are 840 m in length, 1.00–4.28 m in width and 125 m in thickness. The Zn + Pb resources of this orebody exceed 0.4 Mt with ore grades of 2.11–18.26 wt % Zn, 0.18–1.85 wt% Pb, and 7.22–62.24 g/t Ag. Orebody II, the largest orebody in the Lehong deposit, is hosted within the $F_2$ fault and occurs as stratiform to lentiform shapes or as veins paralleling the fault plane (Fig. 2B). This orebody is 2060 m in length, 1.84–29.08 m in width and 282 m in thickness, and its Zn + Pb resources exceed 2.0 Mt with ore grades of 0.8–30.80 wt% Zn, 0.04–15.57 wt% Pb, and 2.40–187.5 g/t Ag. Orebody III is small in scale and occurs as veins hosted within the fault fracture zone (Fig. 2B). It is 100–150 m in length and 1.89–4.88 m in thickness with average ore grades of 4.4 wt% Zn, 0.49 wt% Pb, and 35.69 g/t Ag (Zhou, 2003).

The ore in the Lehong deposit is composed of sulfide ore and a small quantity of oxidized ore. Primary minerals are dominated by sphalerite, galena and pyrite, and hydrothermal dolomite, calcite and minor quartz

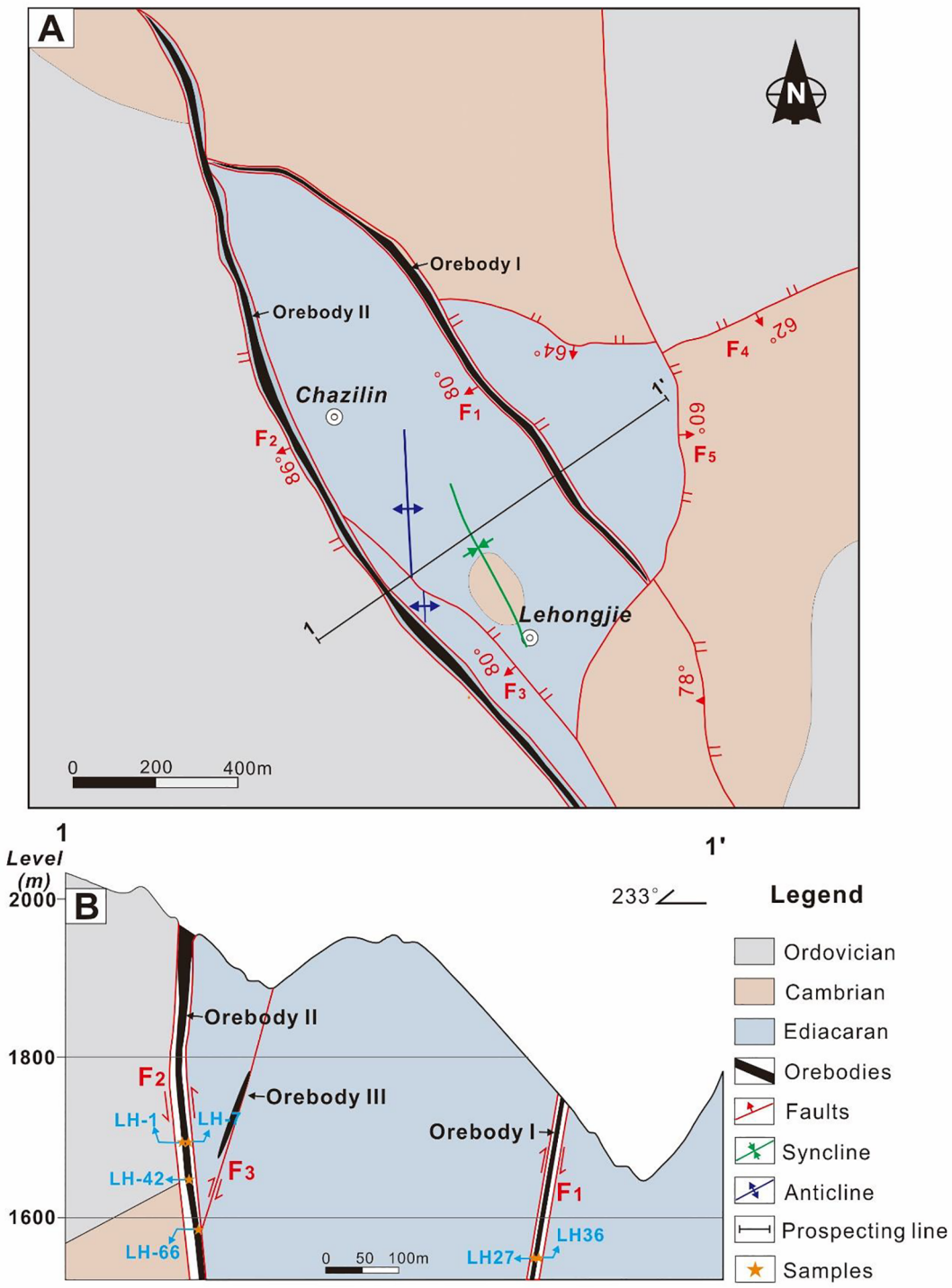


**Fig. 2.** A. Geological sketch map of the Lehong district (modified from Zhou, 2003) showing the distribution of strata and faults. B. Geologic cross-section 1-1′ through the Lehong deposit, revealing the distribution of orebodies, faults and strata (modified from Zhou, 2003).

occur as gangue minerals (Figs. 3 and 4). Moreover, there are a small number of sulfides, i.e., freibergite, chalcopyrite and tennantite, which have been identified by Zhou (2003), but none of these sulfides are observed in this study. The supergene ore is composed of smithsonite, goethite, hemimorphite, hydrozincite and cerussite (Huang, 2003).

The main sulfides in this deposit occur in massive ores (Fig. 3A), breccias (Fig. 3B), disseminated ores (Fig. 3C) and veins. Massive ores are the most common ore texture (Fig. 3A, D, G-H). Sulfide veins are observed from millimeter scale to centimeter scale (Fig. 3B, F). In the disseminated ore, sulfide minerals occur as speckles or single crystals irregularly distributed in the host rocks or in calcite/hydrothermal dolomite (Fig. 3C, I).

The principal ore textures are euhedral-subhedral granular, veinlet-vein filling, cataclastic texture and metasomatic relicts. Sphalerite is the predominant mineral of this deposit, which is characteristically fine-grained and euhedral-subhedral granular (0.02–10 mm). Sphalerite is replaced by galena (Fig. 4D, F, I) or fills in the edges of pyrite (Fig. 4G–H). It also occurs as cataclastic texture (Fig. 4B, D, H). Pyrite usually occurs as euhedral to anhedral fine- to medium-grained minerals (Fig. 4A–B, F-H) and is replaced by sphalerite (Fig. 4A, C). Pyrite

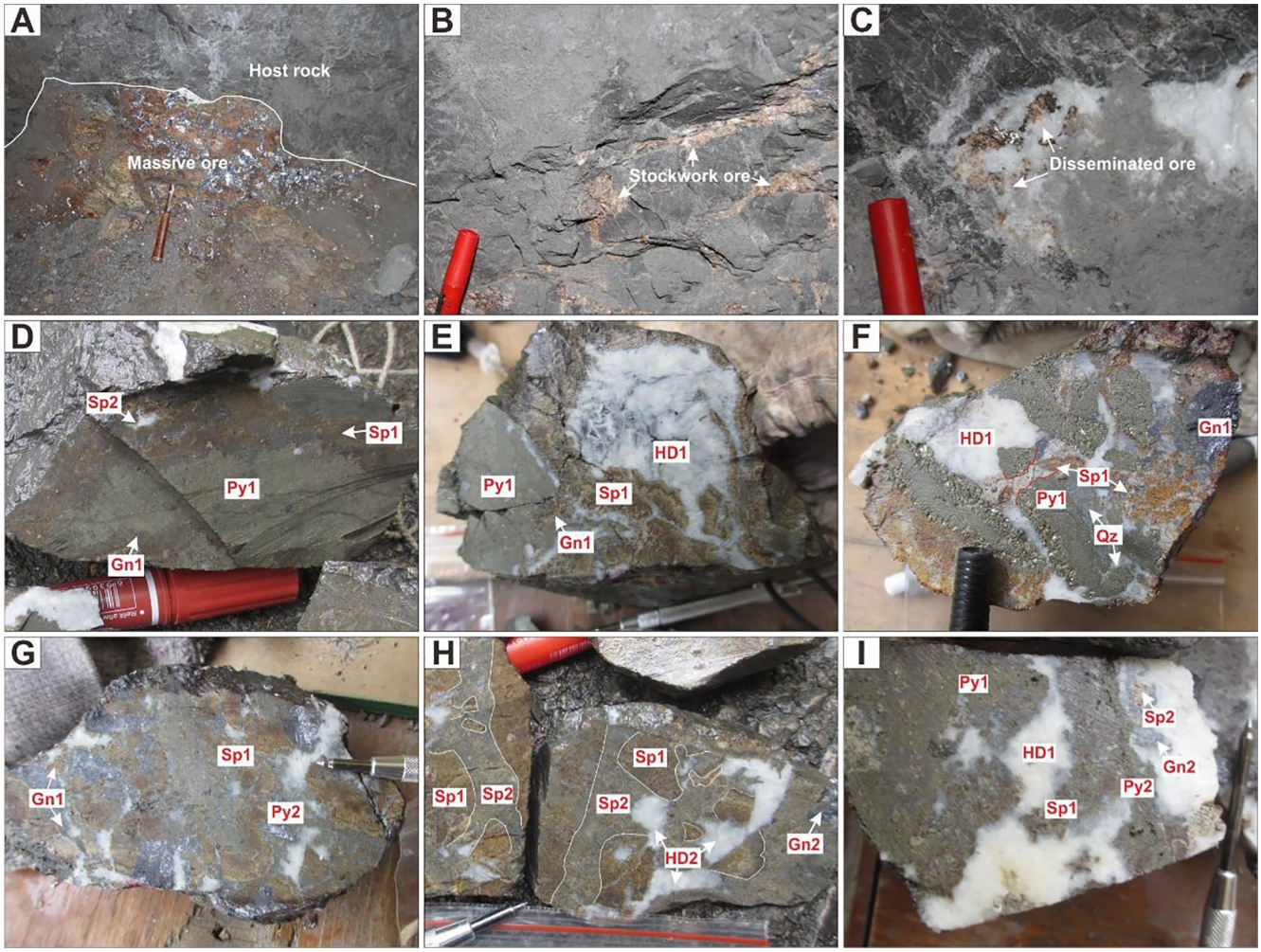


**Fig. 3.** Photographs showing occurrences and texture of the ore at the Lehong deposit. A. A clear contact boundary between lentiform ore and host rock. B. Vein-like sphalerite, galena and hydrothermal dolomite fill the fractures of host rock. C. Disseminated sphalerite irregularly distributed in the host rocks or in hydrothermal dolomite. D. Massive pyrite enclosed by late sphalerite and galena. E. Sphalerite and galena distributed at the edge of massive pyrite and late hydrothermal dolomite in sphalerite fractures. F. Sphalerite crosscutting the early pyrite, and hydrothermal dolomite filling the vugs of sulfides. G. Sphalerite replaced by galena, and late pyrite surrounding the margin of sphalerite. H. Late sphalerite crosscutting the early sphalerite and hydrothermal dolomite fill in the remaining sulfide vugs. I. Early pyrite enclosed by red-brown sphalerite and yellow-brown sphalerite distributed in the hydrothermal dolomite. Mineral abbreviations: Q = quartz, HD = hydrothermal dolomite, Py = pyrite, Sp = sphalerite, Gn = galena. (For interpretation of the references to colour in this figure legend, the reader is referred to the web version of this article.)

veins filling the fractures of sphalerite are also observed (Fig. 4B). Galena is subhedral-anhedral granular and forms veins, which fill the fractures of euhedral pyrite (Fig. 4A) or replace early sphalerite (Fig. 4D, F, I). In addition, calcite and hydrothermal dolomite are mainly veins or veinlet filling in the fractures/vugs of sulfide, i.e., pyrite (Fig. 4G), sphalerite (Fig. 4B, I) and galena (Fig. 4C, E, I).

## 4. Samples and methodology

### 4.1. Sphalerite sample from the Lehong deposit

Ore samples were collected from orebody I (1550 m mining tunnel) and orebody II (1690 m, 1640 m and 1580 m mining tunnels) in the Lehong Zn-Pb deposit. The specimens selected for LA-ICP-MS analysis were biased toward coarse-grained sphalerite generally free of visible inclusions; one-inch polished mounts were prepared from each sample. Scanning electron microscopy (SEM) in backscattered electron mode was used to image the specimens, playing particular attention to mineral inclusions, zoning, compositional inhomogeneities or other textural aspects, all of which may affect trace element distribution.

### 4.2. SEM analysis

Textural and energy dispersive spectroscopy (EDS) analysis of the samples was performed using a field emission scanning electron microscope (JSM-6460 lv, JEOL, Japan) in combination with EDS (TEAM Apex XL, EDAX, America) at the State Key Laboratory of Ore Deposit Geochemistry (SKLOD), Institute of Geochemistry, Chinese Academy of Science (IGCAS). The beam current was 10 nA with an accelerating voltage of 25 kV. Back-scattered electron (BSE) images of ore minerals were obtained in this research. The procedures applied to sphalerite have been detailed in Hu et al. (2018).

### 4.3. LA-ICP-MS spot analysis

LA-ICP-MS analyses of sphalerite were carried out on an Agilent HP-7700 quadrupole ICP-MS instrument at CODES (ARC Centre of Excellence in Ore Deposits, Tasmania, Australia). The instrument was equipped with a high-performance New Wave UP-213 nm solid-state Q-switched laser ablation system. Detailed analytical parameters were described in Cook et al. (2009) and are summarized below.

Spot analyses of sphalerite were performed by laser ablating spots

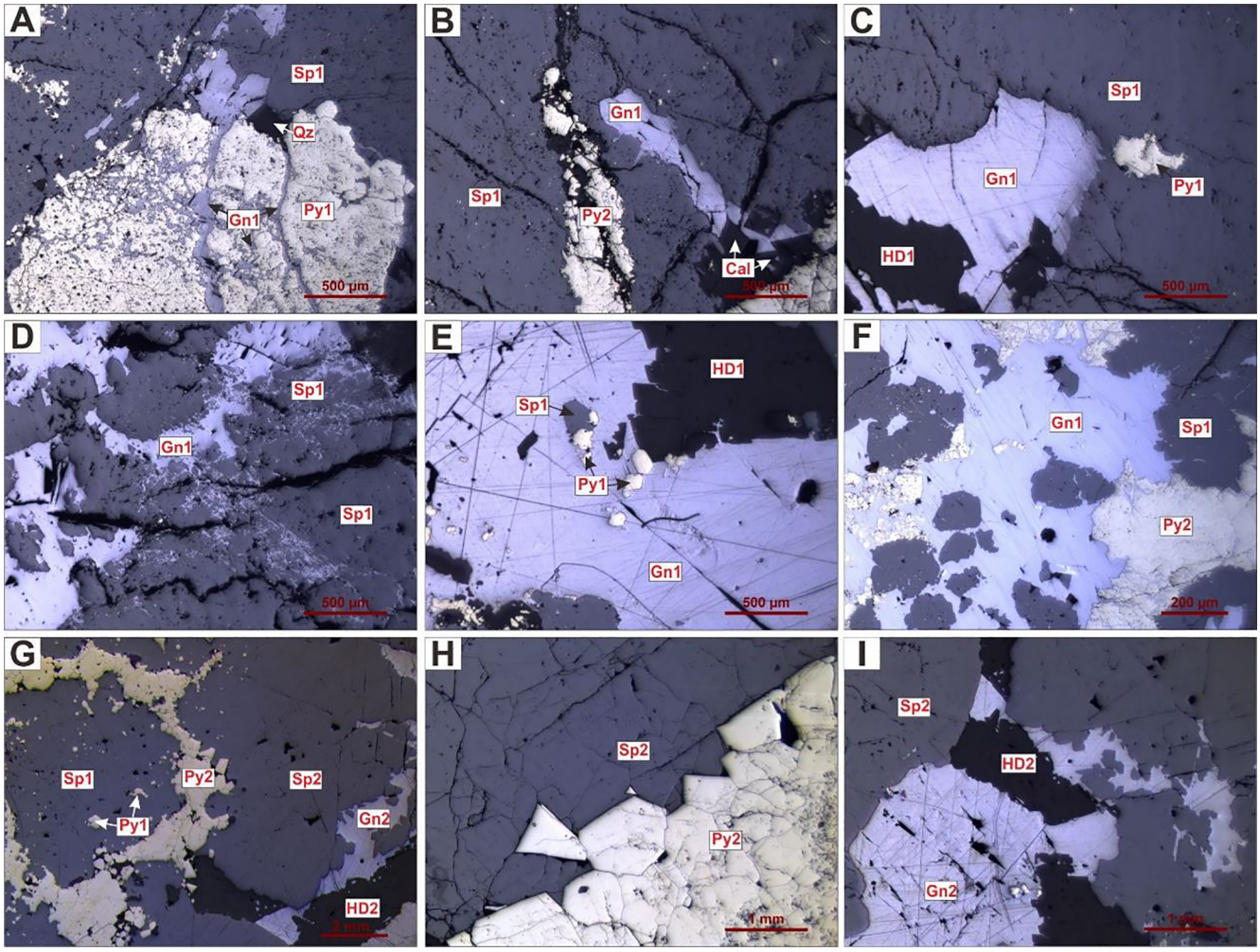


**Fig. 4.** Photomicrographs of sphalerite and representative ore mineral assemblages from the Lehong deposit. A. Galena veinlets filling the fragment of early pyrite. B. Late pyrite fill in the fractures of early sphalerite. C. Early pyrite and galena replaced by sphalerite. D. Early sphalerite replaced by galena. E. Late galena wrapped around early sphalerite and pyrite. F. Late pyrite replacing early sphalerite and galena. G. Early sphalerite wrapped by late pyrite and further replaced or enclosed by late sphalerite. H. Late sphalerite fill at the edge of euhedral pyrite. I. Sphalerite replaced by galena and hydrothermal dolomite fill in the vugs of sulfide. All microphotographs were taken under reflected plane-polarized light. Mineral abbreviations: Cal = calcite, Py = pyrite, Sp = sphalerite, Gn = galena, Cal = calcite, HD = hydrothermal dolomite, Q = quartz.

30 μm in diameter. The repetition rate was 10 Hz, and the laser beam energy was maintained between 5 and 6 J·cm$^{-2}$. The following isotopes were monitored: $^{34}$S, $^{55}$Mn, $^{57}$Fe, $^{65}$Cu, $^{66}$Zn, $^{72}$Ge, $^{107}$Ag, $^{111}$Cd, $^{115}$In, $^{118}$Sn and $^{121}$Sb. The analysis time for each sample was 90 s, consisting of a 30-second background with the laser off and a 60-second analysis with the laser on. The primary calibration standard (STDGL2b2) consists of powdered sulfides doped with certified element solutions and is fused to a lithium borate glass disk developed in-house (Danyushevsky et al., 2011). This standard was analyzed twice every 1.5 h with a 100-μm beam size at 10 Hz to correct for instrument drift.

### 4.4. LA-ICP-MS element distribution mapping

LA-ICP-MS mapping of approximately 0.4 mm$^2$ areas of sphalerite was conducted using a RESOlution 193 nm excimer laser system coupled to an Agilent HP-7700 Quadrupole ICP-MS at CODES (ARC Centre of Excellence in Ore Deposits, Tasmania, Australia). Mapping was carried out by ablating sets of parallel line rasters in a grid across the sample. This method ensured the desired sensitivity of elements of interest as well as adequate spatial resolution depending on the size of the mapped area. The spacing between the lines was adjusted to match the laser spot size. In this analysis, the laser spot size was 25 μm, and the scan speed was maintained at a constant 10 μm/s. A laser repetition of 10 Hz was selected at a constant energy output of 100 mJ. Eight elements were analyzed with the dwell time set to 0.002 s for all elements Thirty seconds of background was acquired by the ICP-MS before each raster was ablated, followed by a delay of 20 s for cell washout, gas stabilization, and computer processing time. Identical rasters were performed on the standard STDGL2b2 sulfide reference material (Danyushevsky et al., 2011). Element maps were compiled and processed using the program Iolite (e.g., Paton et al., 2011) following the method described in Cook et al. (2013) and George et al. (2015).

## 5. Results

### 5.1. Mineral paragenesis

A paragenetic sequence for the Lehong deposit (Fig. 5) was developed from the orefield, hand specimens and thin section samples (Figs. 3 and 4). The hydrothermal mineralization process of the Lehong deposit can be subdivided into three different stages, corresponding well to the mineral assemblages, crosscutting relationships, and previously defined in the literature (Zhao et al., 2018). The main sulfide precipitation occurred in ore stages 1 and 2.

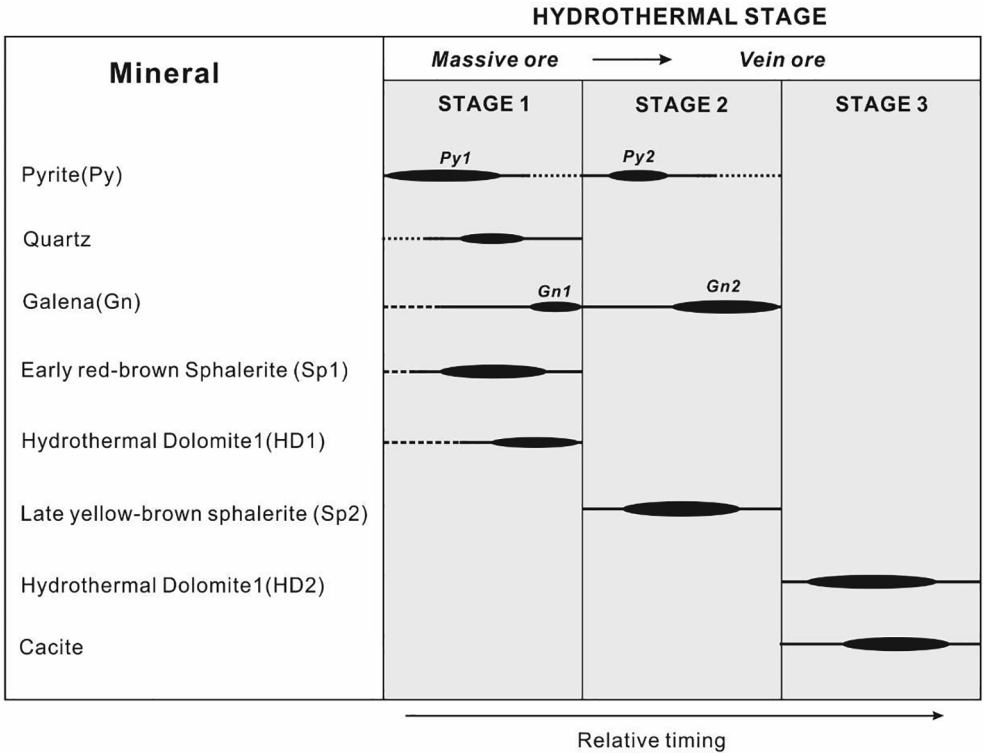


**Fig. 5.** Simplified paragenetic sequence of sulfides, hydrothermal dolomite, and calcite from the Lehong deposit.

Mineralization stage 1: Fe-Zn-Pb-sulfide-quartz

Pyrite 1 and coeval quartz are the earliest hydrothermal minerals in the entire hydrothermal mineralization process. The distribution of this assemblage may have been more extensive in stage 1. Pyrite 1 is medium- to coarse-grained and mainly forms subhedral to anhedral grains (Fig. 4A, C). Quartz accompanies pyrite 1 as fine-grained clear masses (Fig. 3F, 4A). In some samples, pyrite 1 is commonly enclosed by sphalerite 1 (Fig. 3D) and galena 1 (Fig. 4E). Pyrite 1 is commonly replaced by galena 1 (Fig. 3F) or red-brown sphalerite (Fig. 3E). Sphalerite 1 replaces pyrite 1, resulting in irregularly shaped, corroded grain boundaries (Fig. 4A). Fine-grained dispersed pyrite occurs within the sphalerite 1 matrix (Fig. 4C, G). In some cases, sphalerite 1 is enclosed by pyrite 2 as a thin rim among the grain margins (Fig. 4G). Sphalerite 1 crosscutting pyrite 1 is also observed (Fig. 3F). Anhedral galena encloses the sulfide minerals, i.e., pyrite and sphalerite (Fig. 4E). Galena replaces pyrite 1 (Fig. 4A) or sphalerite 1 (Fig. 4D-F, I). Minor hydrothermal dolomite 1 (HD1) is observed in some hand specimens, which fills the vugs of sulfides such as pyrite 1 (Fig. 3F), sphalerite 1 (Fig. 3E) and galena 1 (Fig. 3G).

Mineralization stage 2: Zn-Pb-Fe-sulfide ± hydrothermal dolomite

Pyrite 2 is the earliest mineral of this stage and occurs as euhedral to subhedral grains that extensively replace minerals of the stage 1 assemblage, especially sphalerite 1 (Figs. 3G, 4F–G). In some samples, pyrite 2 fills the cracks of sphalerite 1 (Fig. 4B). Late yellow-brown sphalerite is the most abundant sulfide and occurs as subhedral masses. There is a clear crosscutting relationship between sphalerite 1 and sphalerite 2 (Fig. 3H). In addition, sphalerite 2 replaces or encloses pyrite 2 (Fig. 4G) and forms a clear boundary between pyrite 2 and sphalerite 2 (Fig. 4H). Furthermore, galena 2 commonly occurs anhedral grains and replaces primary sphalerite 2 (Fig. 4I).

Mineralization stage 3: hydrothermal dolomite- calcite

Most hydrothermal dolomite 2 fills the vugs or fractures of the previously described minerals, i.e., pyrite (Figs. 3F, 4G), sphalerite (Figs. 3G, H–I, 4G, I) and galena (Fig. 4E, I). Calcite is the latest mineral, which commonly fills the vugs and/or fractures of sulfides (Fig. 4B) or accompanies hydrothermal dolomite 2.

### 5.2. Trace elements in sphalerite

#### 5.2.1. Sphalerite from different hydrothermal stages

The trace elements in sphalerite analyzed by LA-ICP-MS are summarized in Table 1 for the two identified mineralization stages. The dataset comprises 31 spot analyses in sphalerite 1 and 16 spot analyses in sphalerite 2. The variations in representative elements are illustrated in Fig. 6. In general, the concentrations of most trace elements, including Fe, Cd, Mn, Ge, Cu, Sb, Ag, In and Sn, in the sphalerite of the two hydrothermal stages vary considerably (Table 1).

Sphalerite displays significant Fe concentration in all spot analyses (Table 1). The Fe contents in sphalerite 1 and sphalerite 2 range from 1179 to 36,299 ppm and from 725 to 2529 ppm, respectively, and the Fe content is largely concentrated in sphalerite 1, averaging 8367 ppm.

Sphalerite 1, the early sphalerite, contains higher concentrations of Ge, Cu, Sb and Ag than sphalerite 2. The concentrations of Ge, Cu, Sb and Ag in sphalerite 1 range from 22.9 to 536.0 ppm, 39.4 to 1174.2 ppm, 0.34 to 954.8 ppm, and 8.40 to 297.3 ppm, respectively.

Cd is more concentrated in sphalerite 2 than in sphalerite 1 and ranges from 1571 to 6387 ppm with a mean of 3133 ppm. Interestingly, the concentrations of Mn, In and Sn show no clear difference between sphalerite 1 and sphalerite 2. In all spot analyses, In and Sn concentrations are extremely low, displaying narrow ranges, from 0.01 to 1.15 ppm and 0.04 to 37.24 ppm, respectively. In addition, Mn concentration ranges from 1.18 to 138.4 ppm.

#### 5.2.2. Sphalerite from different mining levels

The trace elements in sphalerite analyzed by LA-ICP-MS are summarized in Table 2 for four different mining levels. The dataset comprises 16 spot analyses in sphalerite from 1690 m, 7 spot analyses in

**Table 1**
LA-ICP-MS results for the sphalerite samples from different hydrothermal stages. Averages are presented as the mean values of all sample geometric means. Minimum (min) and maximum (max) concentrations are extreme values of single sample means.

| | | Mn | Fe | Cu | Ge | Ag | Cd | In | Sn | Sb |
|---|---|---|---|---|---|---|---|---|---|---|
| Sphalerire 1 Red brown sphalerite (n = 31 in 6 samples) | Count | 31 | 31 | 31 | 31 | 31 | 31 | 16 | 25 | 31 |
| | Mean | 27.0 | 8367 | 453.9 | 193.0 | 50.6 | 2820 | 0.10 | 2.47 | 149.8 |
| | S.D. | 27.5 | 8821 | 325.4 | 142.9 | 56.2 | 1178 | 0.28 | 7.48 | 201.8 |
| | Max | 138.4 | 36,299 | 1174.2 | 536.0 | 297.3 | 6686 | 1.15 | 37.24 | 954.8 |
| | Min | 2.8 | 1179 | 39.4 | 22.9 | 8.40 | 574 | 0.01 | 0.04 | 0.34 |
| Sphalerire 2 Yellow brown sphalerite (n = 16 in 4 samples) | Count | 16 | 16 | 16 | 14 | 10 | 16 | 10 | 10 | 16 |
| | Mean | 21.7 | 1397 | 51.2 | 21.8 | 9.2 | 3133 | 0.07 | 3.58 | 11.9 |
| | S.D. | 21.9 | 481 | 48.7 | 18.6 | 10.7 | 1316 | 0.09 | 7.68 | 15.7 |
| | Max | 83.1 | 2529 | 117.9 | 46.4 | 43.6 | 6387 | 0.26 | 25.06 | 44.9 |
| | Min | 1.18 | 725 | 1.23 | 0.42 | 1.54 | 1571 | 0.01 | 0.04 | 0.04 |

sphalerite from 1640 m, 8 spot analyses in sphalerite from 1580 m, and 16 spot analyses in sphalerite from 1550 m. The variations in representative elements are illustrated in Fig. 7. Samples of orebody I are mined from 1550 m; thus, there is no way to analyze the correlation between its concentrations and depth.

The plots of Mn, Ge, Cu and Cd display clear vertical distributions in orebody II (Fig. 7). The highest concentrations of Mn, Ge, Cu and Cd in sphalerite are found in the deeper samples, whereas the upmost sample contains less of these elements. The concentrations of Mn, Ge, Cu and Cd of sphalerite from 1690 m range from 18.5 to 83.1 ppm, 0.42 to 536 ppm, 1.23 to 1174 ppm, and 2399 to 6386 ppm, respectively.

Aside from Mn, Ge, Cu and Cd, the other elements (e.g., Fe, Sb, Ag, In, and Sn) are relatively homogeneous. None of these elements shows significant correspondence with depth.

#### 5.2.3. Element distribution

LA-ICP-MS element mappings of Zn, Pb, Cu, Ge, Ag, Fe, Cd and Sb in sulfide from the Lehong deposit are shown in Fig. 8. All maps show striking compositional heterogeneity, highlighting the differences between sphalerite and galena. Cu, Ge, Fe and Cd are markedly enriched in sphalerite. Conversely, Sb and Ag are relatively enriched in galena. In sphalerite, Ge enrichment closely follows Cu. The LA-ICP-MS mapping also reveals that the presence of Sb is strongly associated with that of Ag, showing that Sb-rich areas are also rich in Ag. In addition, Cd and Zn are relatively uniform in sphalerite and do not display oscillatory zonation; Pb in galena is similar.

## 6. Discussion

### 6.1. Trace element occurrence in sphalerite

Previous studies have demonstrated that bivalent cations, such as Mn, Cd, Co, Cd, and Fe, directly substitute for Zn in the sphalerite lattice (e.g., Cook et al., 2009; Ye et al., 2011). Cook et al. (2012) and Belissont et al. (2014) fully support the incorporation of trivalent and tetravalent cations, such as $Ga^{3+}$, $In^{3+}$ and probably $Sn^{3+}$ or $Sn^{4+}$, via coupled substitutions, i.e., with Cu and Ag. However, the substitution mechanisms of Ge and Sb in sphalerite are more debatable.

#### 6.1.1. The incorporation of Ge and Cu into sphalerite from Lehong

Belissont et al. (2014) proposed coupled substitution mechanisms for Ge and Ag in sphalerite ($3Zn^{2+} \leftrightarrow 2Ag^{+} + Ge^{4+}$) based on the strong correlation between Ge and Ag in sphalerite samples from the Saint-Salvy Zn-Ge deposit, France, leading us to anticipate that analyses with elevated Ge concentration would also clearly feature enrichment in Ag ions. Indeed, the Lehong deposit subset shows no enrichment in Ag ions, and Ge is commonly present at an average concentration three times higher than Ag in all spot analyses (Table 1). Our data reveal an unambiguously expressed non-correlation between mol% Ge and mol% Ag ($R^2 = 0.021$) (Fig. 9A), which could not possibly support the substitution ($3Zn^{2+} \leftrightarrow 2Ag^{+} + Ge^{4+}$) proposed by Belissont et al. (2014). In contrast, there is a strong positive correlation between Ge and Cu in our data ($R^2 = 0.8125$). This result indicates that sphalerite samples rich in Cu are also rich in Ge (Fig. 8), suggesting that these elements are intimately linked in precipitating sphalerite from natural hydrothermal fluids. The mol% Cu is generally present in amounts double those of the mol% Ge, with a trend sub-parallel to $(Cu/Ge)_{mol} = 2$ (Fig. 9B). Such a positive correlation between Ge and Cu may suggest the presence of copper thiogermanates (e.g., briartite, renierite, and/or germanite; Morales-Ruano et al., 1996; Höll et al., 2007); nevertheless, the signals of Ge and Cu are smooth in the time-resolved LA-ICP-MS depth profile of sphalerite, and Ge-bearing micro- and sub-microphases, such as briartite, renierite and germanite, are not observed in the Ge-bearing sphalerite (Ge > 500 ppm) from the Lehong deposit in the high-resolution BSE image (Fig. 10C–F). In addition, none of the Ge-dependent minerals have been observed in the S-Y-G Zn-Pb metallogenic province to date. Thus, we consider that Ge and Cu are incorporated into the sphalerite lattice in the Lehong deposit.

Furthermore, spot concentrations for Ge and Cu show a strong positive correlation in sphalerite from the Lehong deposit. However, many factors, particularly the metal charge in sphalerite and the ionic radius, still have profound influences on the incorporation of trace elements in sphalerite.

First, the metal charge is considered. Ge, like Sn and Pb, has the outer electron configuration [Ar] $3d^{10}4s^{2}4p^{2}$ and generally occurs in the stable form of $Ge^{4+}$ and natural compounds such as sulfide minerals (e.g., argyrodite, canfieldite and germanite), oxides (e.g., argutite) and hydroxides (e.g., stottite; Höll et al., 2007), whereas $Ge^{2+}$ exists only in synthetic compounds that are usually unstable under atmospheric conditions (Bernstein, 1985; Rosenberg, 2009). Moreover, Ge and Cu K-edge X-ray absorption near edge spectra (XANES) have confirmed the presence of $Ge^{4+}$ and $Cu^{+}$, respectively, in the tetravalent site of Ge-rich sphalerite from Tres Marias (Cook et al., 2015). Similar oxidation states of Ge and Cu have been proposed for sphalerite from the Saint-Salvy deposit, France, as well as that of the Kipushi deposit, Congo, by Belissont et al. (2016). Currently, we find no literature verifying the presence of $Cu^{2+}$, which are incorporated into the sphalerite lattice. Therefore, we infer that the oxidation states of Ge and Cu in sphalerite from the Lehong deposit are likely +4 and +1, respectively.

Another key factor controlling the incorporation of trace elements in sphalerite is the ionic radius. The ionic radii of $Ge^{4+}$ and $Cu^{+}$ are 0.39 Å and 0.60 Å in the tetrahedral configuration (Shannon, 1976), respectively, and close to the $Zn^{2+}$ ionic radius (0.60 Å), suggesting that $Ge^{4+}$ and $Cu^{+}$ are easily incorporated into sphalerite by replacing $Zn^{2+}$.

Considering the correlation between Ge and Cu, metal oxidation, and ionic radius, our results strongly support a coupled substitution such as $3Zn^{2+} \leftrightarrow 2Cu^{+} + Ge^{4+}$.

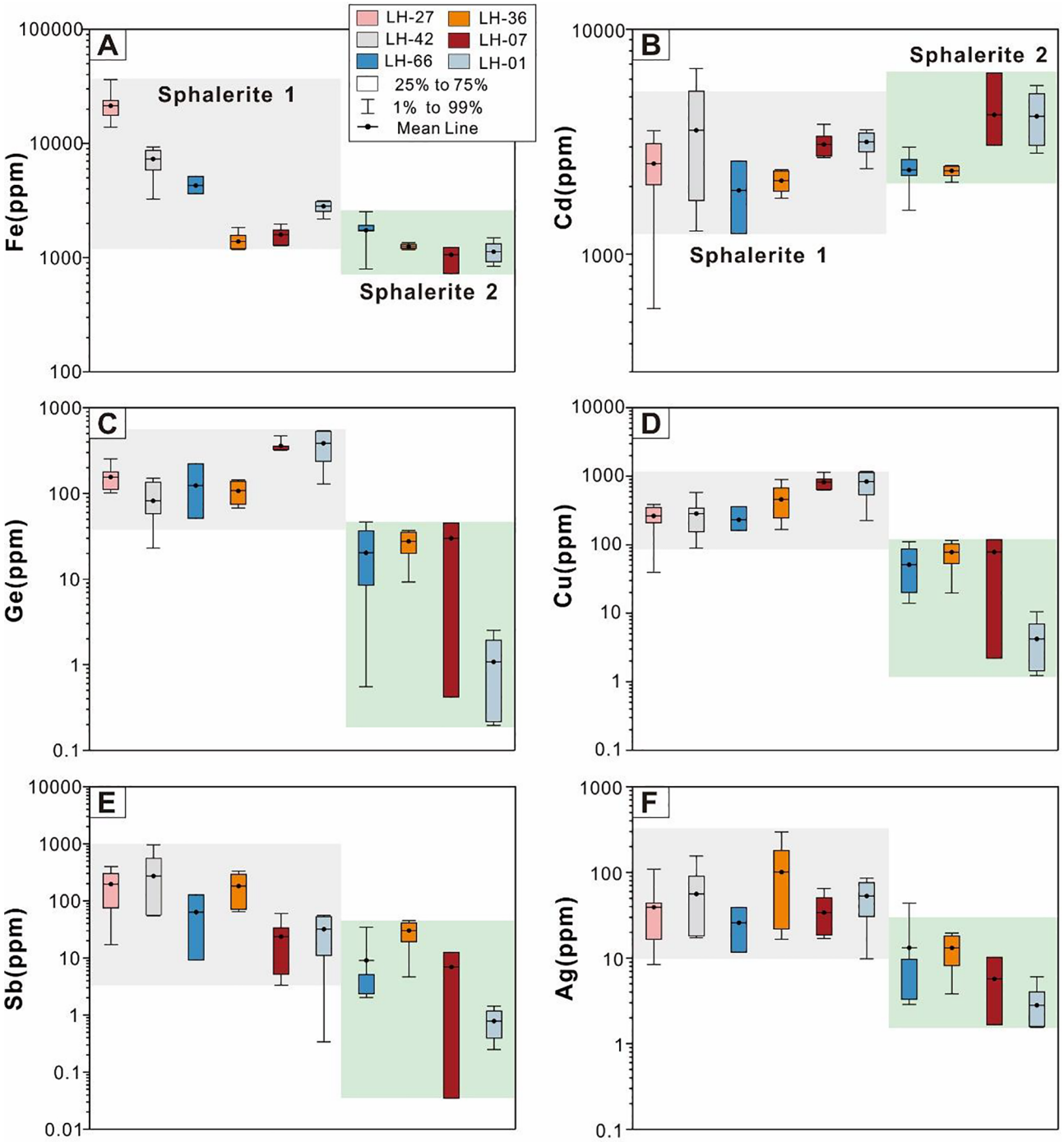


**Fig. 6.** Box-and-whisker plots of the trace element results of sphalerite from the Lehong deposit, grouped into the two stages sphalerite (Sphalerite 1 and Sphalerite 2).

*6.1.2. The incorporation of Sb and Ag into sphalerite from Lehong*

It is well recognized that Sb and Ag are incorporated into galena via the coupled substitution $2Ag^{+} + Sb^{3+} \leftrightarrow 2Pb^{2+}$ (Wernick 1960; Amcoff 1976; Sharp and Buseck 1993; Costagliola et al. 2003; Chutas et al. 2008; Renock and Becker 2011; George et al., 2015); however, Sb and Ag occurrence in sphalerite are still inconclusive. Cook et al. (2009) considered that Sb in sphalerite is mostly interpreted in terms of micro-scale inclusions of galena or Ag-Sb-bearing minerals and that Ag occurs as micro-scale inclusions or as solid solution. If the hypothesis is correct, micro-scale inclusions of galena or Ag-Sb-bearing minerals should be observed in the sphalerite from Lehong. In contrast, in Lehong sphalerite, the signals of Sb, Ag and Pb are smooth and show no abnormal peaks of Sb and Ag in the time-resolved LA-ICP-MS depth profile (Fig. 10B), and microphase inclusions of galena or Ag-Sb-bearing minerals are not observed in the high-resolution BSE images (Fig. 10C–F). Furthermore, coordinate variations in Sb and Ag are displayed in LA-ICP-MS element distribution mapping, and the Sb enrichment area is also enriched in Ag (Fig. 8). Thus, all evidence suggests that Sb and Ag are incorporated into the sphalerite lattice at the Lehong deposit.

Expressed as mol% on a binary plot, the correlation between Sb and Ag has a trend subparallel to the molar ratio $(Sb/Ag)_{mol} = 1$ (Fig. 9C). Moreover, the Sb contents in spot analysis data of sphalerite from the Lehong deposit are nearly equal to those of Ag and much smaller than

**Table 2**
LA-ICP-MS results for the sphalerite samples from different mining levels. Averages are presented as the mean values of all sample geometric means. Minimum (min) and maximum (max) concentrations are extreme values of single sample means.

| Orebody | Level(m) | | Mn | Fe | Cu | Ge | Ag | Cd | In | Sn | Sb |
|---|---|---|---|---|---|---|---|---|---|---|---|
| | | Count | 16 | 16 | 16 | 14 | 16 | 16 | 9 | 9 | 16 |
| II | 1690 | Mean | 42.6 | 1742 | 480.2 | 247.2 | 25.7 | 3557 | 0.04 | 0.85 | 16.9 |
| | (2 samples) | S.D. | 19.0 | 753 | 462.8 | 202.7 | 28.1 | 1102 | 0.06 | 1.60 | 21.4 |
| | | Max | 83.1 | 3151 | 1174.2 | 536.0 | 85.5 | 6387 | 0.17 | 4.57 | 60.6 |
| | | Min | 18.5 | 725 | 1.23 | 0.42 | 1.54 | 2399 | 0.00 | 0.04 | 0.04 |
| | | Count | 7 | 7 | 7 | 7 | 7 | 7 | 4 | 6 | 7 |
| II | 1640 | Mean | 11.6 | 7303 | 286.0 | 81.8 | 55.9 | 3559 | 0.04 | 1.92 | 272.9 |
| | (1 samples) | S.D. | 6.22 | 2085 | 157.3 | 45.1 | 50.4 | 1917 | 0.05 | 2.54 | 349.5 |
| | | Max | 21.3 | 9309 | 581.5 | 151.0 | 155.8 | 6686 | 0.11 | 6.96 | 954.8 |
| | | Min | 3.53 | 3253 | 89.2 | 22.9 | 17.3 | 1269 | 0.01 | 0.09 | 56.0 |
| | | Count | 8 | 8 | 8 | 8 | 8 | 8 | 4 | 6 | 8 |
| II | 1580 | Mean | 4.55 | 2687 | 118.8 | 59.0 | 17.9 | 2200 | 0.08 | 5.45 | 29.6 |
| | (1 samples) | S.D. | 3.30 | 1456 | 115.9 | 72.8 | 16.3 | 586 | 0.12 | 9.96 | 43.7 |
| | | Max | 9.76 | 5139 | 360.5 | 221.6 | 43.6 | 2995 | 0.26 | 25.06 | 127.0 |
| | | Min | 1.18 | 794 | 14.1 | 0.55 | 2.87 | 1235 | 0.01 | 0.09 | 2.02 |
| | | Count | 16 | 16 | 16 | 16 | 16 | 16 | 9 | 14 | 16 |
| I | 1550 | Mean | 24.0 | 11,328 | 266.1 | 111.4 | 48.1 | 2383 | 0.15 | 3.26 | 151.1 |
| | (2 samples) | S.D. | 31.5 | 11,422 | 213.0 | 66.4 | 71.4 | 726 | 0.38 | 9.80 | 134.7 |
| | | Max | 138.4 | 36,299 | 898.3 | 253.4 | 297.3 | 3539 | 1.15 | 37.24 | 398.7 |
| | | Min | 5.27 | 1179 | 19.7 | 9.22 | 3.82 | 574 | 0.00 | 0.04 | 4.67 |

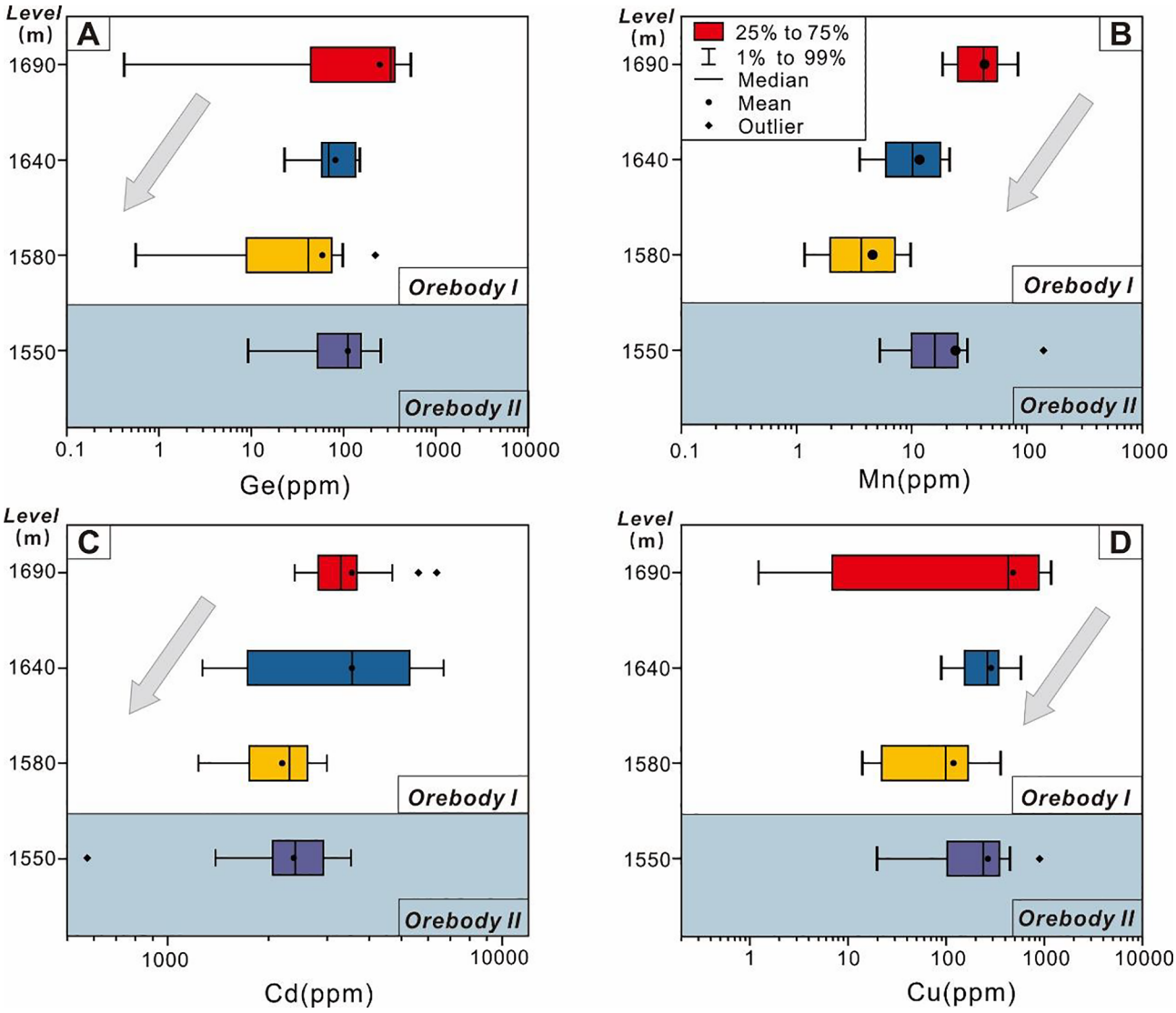


**Fig. 7.** Box-and-whisker plots of the trace elements (Mn, Ge, Cd and Cu) in sphalerite from different levels and orebodies of the Lehong deposit.

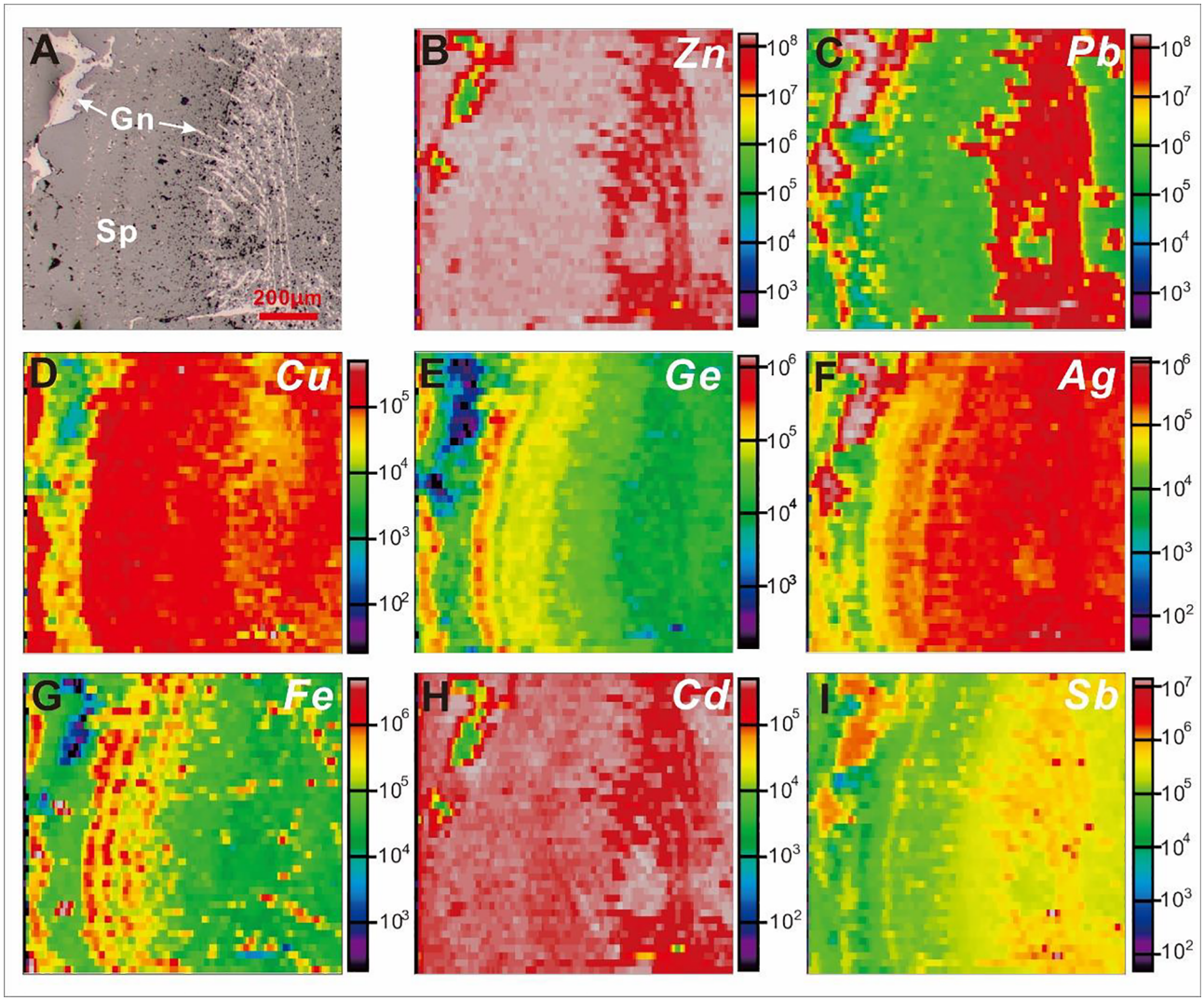


**Fig. 8.** Elemental maps generated with LA-ICP-MS show the distribution of selected trace elements in sphalerite from sample LH-01, Lehong deposit. A. Reflected light photomicrograph of mapped sphalerite crystals that enclose several galena grains. B–I. Different elements (Zn, Pb, Cu, Ge, Ag, Fe, Cd, and Sb, respectively) of LA-ICP-MS maps. Mineral abbreviations: Sp = sphalerite, Gn = galena,

those of Cu. Interestingly, in some high-Cu sphalerite samples, Sb contents are considerably higher than Ag contents. Assuming that such a coupled substitution mechanism can account for the total Ag incorporation into sphalerite, Sb has likely been involved in other substitution mechanisms to reach these concentrations, particularly for Cu, In and Sn (Fig. 9D). A similar well-defined Sb-Ag correlation has been reported for different genetic Zn-Pb deposits in southern China by Ye et al. (2011).

Olsen et al. (2016) showed that $Sb^{3+}$ is the dominant valence state in hydrothermal solutions and that Sb-bearing species are dependent on the pH and sulfide concentration of the solution. Han et al. (2017) show that $Sb^{3+}$ commonly occurs in iron sulfide. In addition, $Sb^{3+}$ is generally present in most Sb minerals, i.e., stibnite, chalcostibite and tetrahedrite. Thus, the oxidation state of Sb in sphalerite is likely the +3 state. Ag likely exists in the +1 state, which has been interpreted (Cook et al., 2009; Ye et al., 2011; George et al., 2016) as solid solution in sphalerite.

Concerning the ionic radius, the ionic radii of $Sb^{3+}$ and $Ag^{+}$ are 0.76 Å and 1.00 Å, respectively, in the tetrahedral configuration (Shannon, 1976) and close to the $Zn^{2+}$ ionic radius (0.60 Å), indicating that $Sb^{3+}$ and $Ag^{+}$ are apt to be incorporated into sphalerite by replacing $Zn^{2+}$.

As mentioned above, the coupled substitution may thus be more accurately expressed as $2Zn^{2+} \leftrightarrow Ag^{+} + Sb^{3+}$.

### *6.1.3. The coupled substitution between trivalent and tetravalent cations and monovalent cations in sphalerite from Lehong*

Johan (1988) proposed that a coupled substitution mechanism would result in trivalent and tetravalent element (including $Sb^{3+}$, $In^{3+}$, $Sn^{4+}$, and $Ge^{4+}$) enrichments with respective monovalent cations (i.e., Cu and Ag) in sphalerite. A strong correlation between Sb + Ge + In + Sn (trivalent and tetravalent cations) and Cu + Ag (monovalent cations) along the 1/1 M ratio (Fig. 11) highlights a general coupled substitution for trace elements incorporated into sphalerite. Interestingly, in all spot analyses, the monovalent cation concentrations (Cu and Ag) approach the sum of all trivalent and tetravalent cations. It is suggested that the monovalent cations provide charge balance in all coupled substitutions and could take the responsibility for a large number of trivalent and tetravalent cations, especially In, Sn, Sb, and Ge, incorporated into sphalerite. In addition, the scattered data are slightly below the 1/1 M ratio line (Fig. 11) because there is no analyses of Ga concentration.

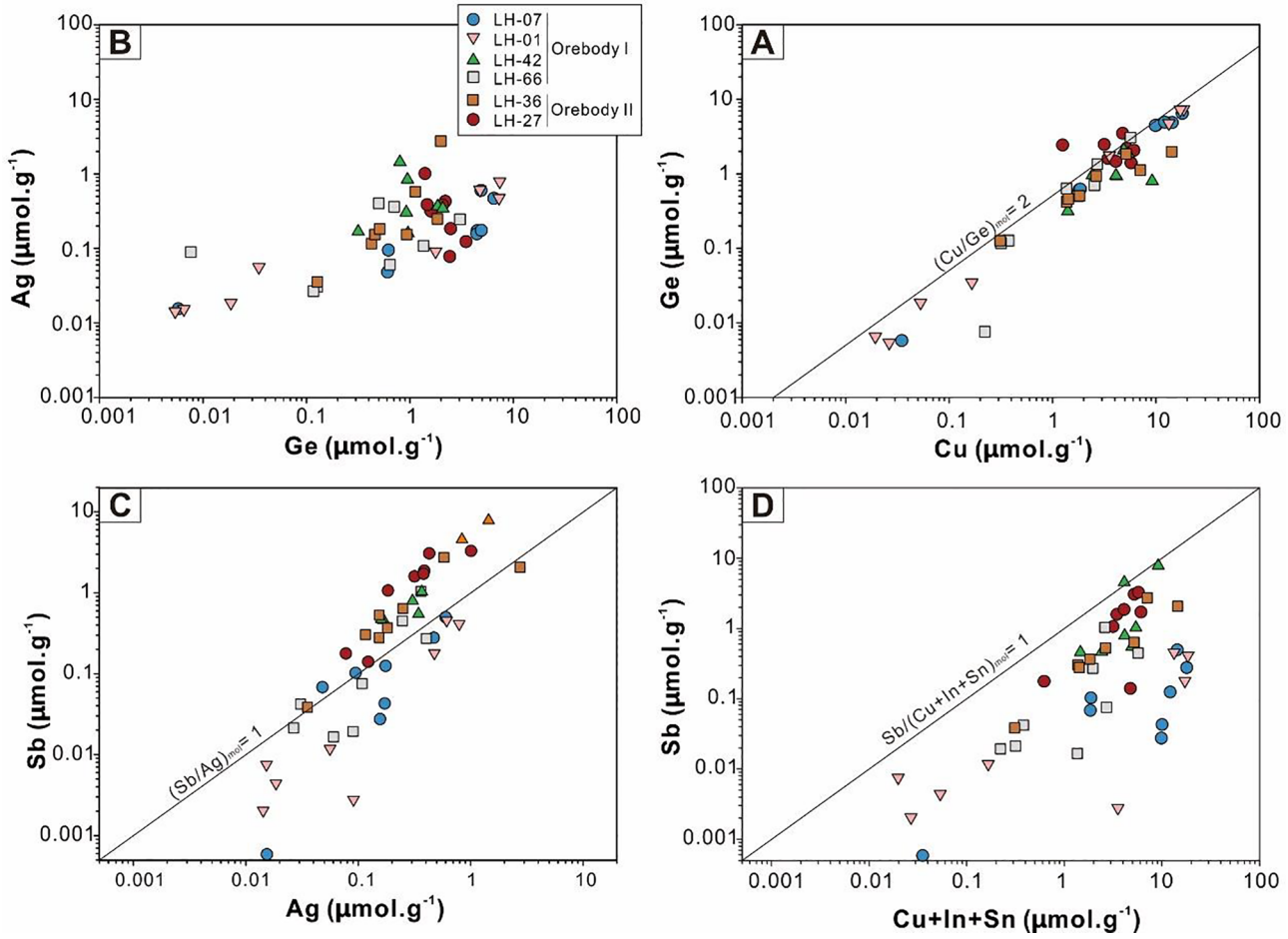


**Fig. 9.** Binary correlation plots, trend lines, and suggested coupled substitution mechanisms. A. The correlation between Ag and Ge. B. The correlation between Cu and Ge, with a trend sub-parallel to $(Cu/Ge)_{mol} = 2$. C. Ag correlated with Sb with a trend sub-parallel to the $(Ag/Sb)_{mol} = 1$ line. D. The correlation between Cu + In + Sn and Sb, with a trend sub-parallel to the $Sb/(Cu + In + Sn)_{mol} = 1$ line.

### 6.2. Significance of trace element trends in evolution of hydrothermal fluids

Fe and other trace elements, such as Ge, Cu, Sb, Ag, Cd, In, Sn and Mn, can partition from hydrothermal fluids and be incorporated into the sphalerite lattice by substituting for $Zn^{2+}$ during crystal growth or recrystallization (Cook et al., 2009, 2012; Ye et al., 2011,2016; Murakami and Ishihara, 2013; Belissont et al., 2014; Wei et al., 2018a and this study). The incorporation and distribution of trace elements in sphalerite is controlled by the geochemical properties of elements, crystal-fluid partition coefficients and bulk concentrations in hydrothermal fluid (e.g., Belissont et al., 2016; Bauer et al., 2019). Thus, the sphalerite that formed in different stages in the Lehong deposit, combined with previously published fluid inclusion data, can be studied to provide useful information on the physical chemistry and evolution process of hydrothermal fluids.

In the Lehong deposit, both types of sphalerite contain variable concentrations of siderophile and chalcophile elements (e.g., Ge, Cu, Sb, Ag, Cd, and Fe), suggesting that hydrothermal fluids were heterogeneous in composition. The early red-brown sphalerite intergrowths with pyrite and quartz are relatively enriched in Fe, Ge, Cu, Sb and Ag (Fig. 6). The reported temperatures of mineralization at the Lehong deposit suggest that the early sphalerite formed between 217.8 and 292.2 °C (Zhao et al., 2018). The fluid inclusions dataset and newly obtained trace element concentrations in early sphalerite indicate that the early intermediate- to low-temperature hydrothermal fluid tended to precipitate Lehong sphalerite enriched in Fe, Ge, Cu, Sb and Ag. Late sphalerite is characterized by slightly elevated Cd and distinctly decreased Fe, Ge, Cu, Sb and Ag (Fig. 6) and coexists with galena and hydrothermal dolomite. Microthermometry of fluid inclusions indicates that the formation temperature of late sphalerite at the Lehong deposit ranges from 140.4 °C to 227.4 °C (Zhao et al., 2018). This evidence suggests that sphalerite enriched in Cd was produced in relatively low-temperature hydrothermal systems.

In summary, sphalerite enriched in Fe, Ge, Cu, Sb and Ag was prone to form in the early hydrothermal fluid; sphalerite with elevated Cd was preferentially produced in the late hydrothermal fluid as the hydrothermal fluid temperature decreased at Lehong.

### 6.3. Coupling of Fe and Ge in sphalerite during evolution of hydrothermal fluids

There are few but sufficient study data on the behavior of Ge in hydrothermal fluid systems. Ge is slightly enriched in silicate minerals of late magmatic differentiates and late hydrothermal fluids on the basis of previous studies (Bernstein, 1985; Höll et al., 2007). Sphalerite is one of the main Ge carriers and provides a by-product in sphalerite processing (Höll et al., 2007; Cook et al., 2009). Kelley et al. (2004) demonstrated that late-precipitating, Fe-poor sphalerite is relatively enriched in Ge. In the Lehong deposit, however, Fe and Ge are enriched in the early red-brown sphalerite and depleted in the late yellow-brown sphalerite. Although a profound understanding of the controls on Ge enrichment in early sphalerite requires reliable experimental thermodynamic study, *in situ* LA-ICP-MS data from sphalerite of the Lehong deposit show that the Cu contents in all crystals of the analyzed sample

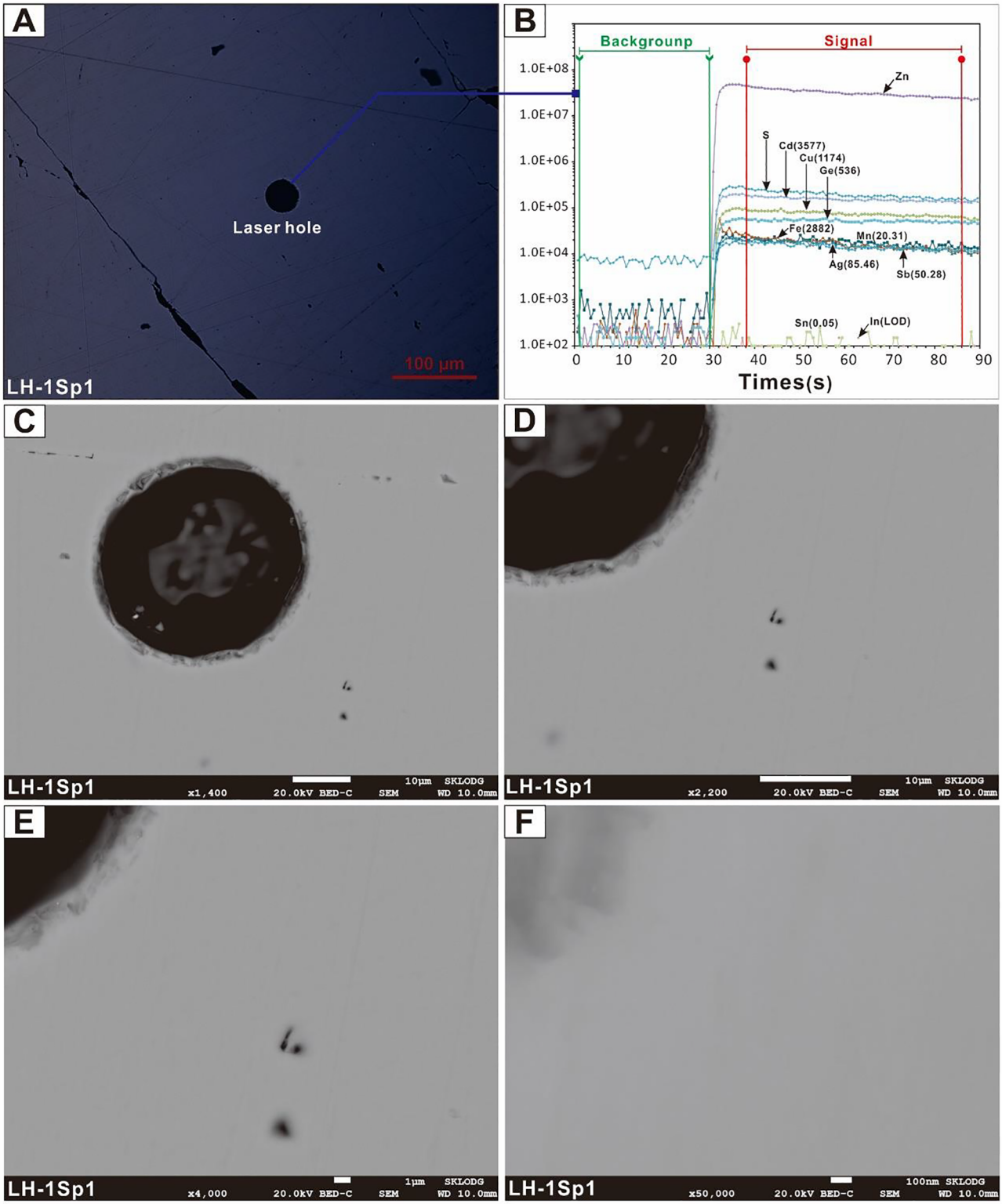


**Fig. 10.** A. The laser hole of Ge-bearing sphalerite (LH-01Sp1) from Lehong. B. The time-resolved LA-ICP-MS depth profiles of LH-01Sp1. C-F. Different magnification of backscattered electron (BSE) images around the laser hole (C. BSE image enlarged 1400 times. D. BSE image enlarged 2200 times. E BSE image enlarged 4000 times. F. BSE image enlarged 50,000 times).

are nearly double those of Ge. It is suggested that the increase in Cu concentration would promote the incorporation of Ge during Lehong sphalerite precipitation from hydrothermal fluids (Johan, 1988). Moreover, in sphalerite from the Saint-Salvy deposit, a high Ge content (~2600 pm, Belissont et al., 2014) related to the Cu concentration has been reported (Belissont et al., 2016). Thus, Cu enrichment in early sphalerite may be a key controlling factor for increasing Ge concentration, further resulting in the coupling of Fe and Ge in sphalerite during the evolution of hydrothermal fluids.

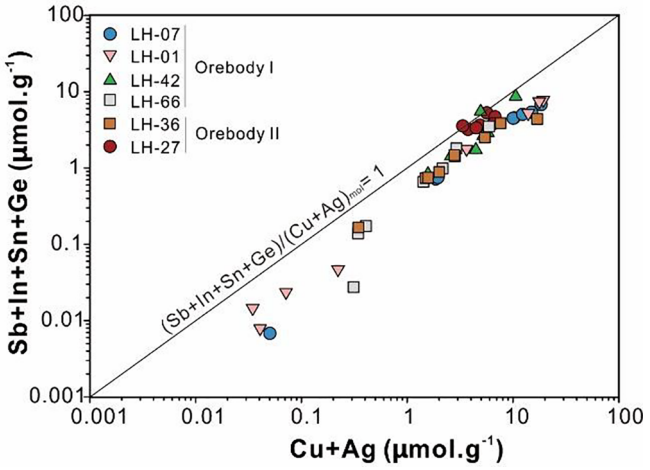


**Fig. 11.** The strong correlation between Sb + Ge + In + Sn (trivalent and tetravalent cations) and Cu + Ag (monovalent cations) along the 1/1 M ratio highlights a general coupled substitution mechanism for trace elements in sphalerite.

### *6.4. Vertical zoning of Mn, Ge, Cu and Cd in sphalerite – Implications for mineral exploration*

Our study has shown that shallow sphalerite is more depleted in Mn, Ge, Cu and Cd more than sphalerite at depth. There is a clear upward trend among Mn, Ge, Cu and Cd in sphalerite with increasing vertical depth at Lehong (Fig. 7). This view has significant implications for Zn-Pb mineral exploration in this orefield because trace elements, such as Mn, Ge, Cu and Cd, in sphalerite have clear vertical zoning. Similar sphalerite enriched in Ge, Cd and Cu in the deep part has been reported from carbonate-hosted Zn-Pb deposits (Ye et al., 2016; Yuan et al., 2018; Hu et al., 2019).

Although several aspects of the vertical zoning of Mn, Ge and Cd in sphalerite remain unclear, the predictive model suggests that deep sphalerite in the orebody is more enriched in Mn, Ge, Cd and Cu than sphalerite at shallow levels and may be a potential exploration target.

In the Yangtze Block, carbonate-hosted Zn-Pb deposits are widespread in the platform carbonate sequence, such as the S-Y-G Zn-Pb metallogenic province (Hu et al., 2018), including more than 400 carbonate-hosted Zn-Pb deposits that formed during the Late Triassic (~200 to 230 Ma) (Zhang et al., 2015; Hu et al., 2017). One significant feature is that all deposits are epigenetic, and their orebodies are hosted within the fault fracture zone (Huang et al., 2004; Han et al., 2007). As mentioned above, the deep sphalerite is more enriched in Ge, Cu and Cd than sphalerite in the shallow zone, as the orebody hosted within the fault fracture zone. The Daliangzi deposit in southwestern Sichuan Province may be such an example; trace elements, such as Ge, Cu and Cd, in sphalerite generally elevate with increasing depth from shallow to deep (Yuan et al., 2018). Moreover, the newly discovered Nayongzhi and Niugongtang deposits in northwestern Guizhou Province indicate that this district still presents wide prospects in search for Zn-Pb deposits. Thus, the vertical zoning of Mn, Ge and Cd in sphalerite may be a potential tool for Zn-Pb mineral exploration.

## 7. Conclusions

The main findings of this study are as follows:

1. LA-ICP-MS element mapping and SEM study show that no Ge-bearing micro-minerals are observed in the Lehong deposit. Strong binary correlations between Cu and Ge and between Ag and Sb suggest the coupled substitutions $3Zn^{2+} \leftrightarrow 2Cu^{+} + Ge^{4+}$ and $2Zn^{2+} \leftrightarrow Ag^{+} + Sb^{3+}$. Additionally, in all spots, the monovalent elements, i.e., Cu and Ag, approach the sum of all trivalent and tetravalent elements. It is suggested that the monovalent cations may provide charge balance in all coupled substitutions responsible for incorporating a wide range of trivalent and tetravalent cations, especially In, Sn, Sb, and Ge, in sphalerite at Lehong.
2. Trace elements in sphalerite from the two mineralization stages are significantly different. Sphalerite 1 is more enriched in Fe, Ge, Cu, Sb and Ag than sphalerite 2. Fluid inclusion study and the newly obtained trace elements of sphalerite from different hydrothermal stages indicate that trace elements in sphalerite may have the potential to record the evolution of hydrothermal fluids.
3. Fe and Ge are enriched in early sphalerite and depleted in late sphalerite, which points toward decoupled behavior of Fe and Ge in the Lehong deposit. We consider that increasing the Cu concentration would promote the incorporation of Ge in early sphalerite during the evolution of hydrothermal fluids.
4. Mn, Ge, Cu and Cd display clear vertical distribution in orebody II at Lehong, similar to those of carbonate-hosted Zn-Pb deposits (e.g., Daliangli and Fule deposits) in the S-Y-G metallogenic province, which may provide a potential tool for Zn-Pb mineral exploration in this district.

## Acknowledgements

This research project was jointly supported by the National Key Research and Development Project of China (No. 2017YFC0602502), the National Natural Science Foundation of China (Grant No. 41673056, 41430315), and the Science and Technology Key Project of Guizhou Province ([2017]1421). We thank Dr. Ivan Belousov, Dr. Paul Olin, and Dr. Sahra Gilbert (CODES, University of Tasmania) for their assistance with LA-ICP-MS analysis and Dr. Shaohua Dong (SKLOD, Institute of Geochemistry) for her assistance with SEM analysis. We express our appreciation to Editor Franco Pirajno, Guest Editor Hanjie Wen, Dr. Zhiyong Zhu, and an anonymous reviewer for their insightful comments that greatly improved the quality of the manuscript.

## References

Amcoff, O., 1976. The solubility of silver and antimony in galena. Neues Jahrbuch für Mineralogie Monatshefte 6, 247–261.
Bauer, M.E., Burisch, M., Ostendorf, J., Krause, J., Seifert, T., Gutzmer, J., 2019. Trace element geochemistry of sphalerite in contrasting hydrothermal fluid systems of the Freiberg district, Germany: insights from LA-ICP-MS analysis, near-infrared light microthermometry of sphalerite-hosted fluid inclusions, and sulfur isotope geochemistry. Miner. Deposita 52 (2), 237–262.
Belissont, R., Boiron, M.C., Luais, B., Cathelineau, M., 2014. LA-ICP-MS analyses of minor and trace elements and bulk Ge isotopes in zoned Ge-rich sphalerites from the Noailhac – SaintSalvy deposit (France): insights into incorporation mechanisms and ore deposition processes. Geochim. Cosmochim. Acta 126, 518–540.
Belissont, R., Muñoz, M., Boiron, M.C., Luais, B., Mathon, O., 2016. Distribution and oxidation state of Ge, Cu and Fe in sphalerite by μ-XRF and K-edge μ-XANES: insights into Ge incorporation, partitioning and isotopic fractionation. Geochim. Cosmochim. Acta 177, 298–314.
Bernstein, L.R., 1985. Germanium geochemistry and mineralogy. Geochim. Cosmochim. Acta 49 (11), 2409–2422.
Bonnet, J., Cauzid, J., Testemale, D., Kieffer, I., Proux, O., Lecomte, A., Bailly, L., 2017. Characterization of germanium speciation in sphalerite (ZnS) from central and eastern Tennessee, USA, by X-ray absorption spectroscopy. Minerals 7 (5), 79.
Chutas, N.I., Kress, V.C., Ghiorso, M.S., Sack, R.O., 2008. A solution model for high temperature PbS-$AgSbS_2$-$AgBiS_2$ galena. Am. Mineral. 93, 1630–1640.
Cook, N.J., Ciobanu, C.L., Brugger, J., Etschmann, B., Howard, D.L., De Jonge, M.D., Ryan, C., Paterson, D., 2012. Determination of the oxidation state of Cu in substituted Cu In-Fe-bearing sphalerite via μ-XANES spectroscopy. Am. Mineral. 97, 476–479.
Cook, N.J., Ciobanu, C.L., Meria, D., Silcock, D., Wade, B.P., 2013. Arsenopyrite-pyrite association in an orogenic gold ore: tracing mineralization history from textures and trace elements. Econ. Geol. 108, 1273–1283.
Cook, N.J., Ciobanu, C.L., Pring, A., Skinner, W., Shimizu, M., Danyushevsky, L., Saini-Eidukat, B., Melcher, F., 2009. Trace and minor elements in sphalerite: a LA-ICPMS study. Geochim. Cosmochim. Acta 73 (16), 4761–4791.
Cook, N.J., Etschmann, B., Ciobanu, C.L., Geraki, K., Howard, D., Williams, T., Rae, N., Pring, A., Chen, G., Johannessen, B., Brugger, J., 2015. Distribution and substitution mechanism of Ge in a Ge-(Fe)-bearing sphalerite. Minerals 5 (2), 117–132.
Costagliola, P., Di Benedetto, F., Benvenuti, M., Bernardini, G.P., Cipriani, C., Lattanzi, P.F., Romanelli, M., 2003. Chemical speciation of Ag in galena by EPR spectroscopy. Am. Mineral. 88, 1345–1350.
Cugerone, A., Cenki-Tok, Bénédicte, Chauvet, A., Le Goff, E., Bailly, L., Alard, O., Allard,

M., 2018. Relationships between the occurrence of accessory Ge-minerals and sphalerite in Variscan Pb-Zn deposits of the Bossost anticlinorium, French Pyrenean Axial Zone: chemistry, microstructures and ore-deposit setting. Ore Geol. Rev. 95, 1–19.
Danyushevsky, L., Robinson, P., Gilbert, S., Norman, M., Large, R., McGoldrick, P., Shelley, M., 2011. Routine quantitative multi-element analysis of sulphide minerals by laser ablation ICP-MS: standard development and consideration of matrix effects. Geochem. Explor. Environ. Anal. 11, 51–60.
Frenzel, M., Hirsch, T., Gutzmer, J., 2016. Gallium, germanium, indium, and other trace and minor elements in sphalerite as a function of deposit type — a meta-analysis. Ore Geol. Rev. 76 (9), 52–78.
George, L., Cook, N.J., Ciobanu, C.L., 2016. Partitioning of trace elements in co-crystallized sphalerite-galena-chalcopyrite hydrothermal ores. Ore Geol. Rev. 77, 97–116.
George, L., Cook, N.J., Ciobanu, C.L., Wade, B.P., 2015. Trace and minor elements in galena: a reconnaissance LA-ICP-MS study. Am. Mineral. 100 (2–3), 548–569.
Halfon, J., Rosique, A., 1973. Comparaison des elements “entraces” dans les blendes du filon et les blendes du stratiforme de Saint-Salvy (81). Bull. BRGM 5, 403–432(2), II.
Han, R.S., Liu, C.Q., Huang, Z.L., Chen, J., Ma, D.Y., Lei, L., Ma, G.S., 2007. Geological features and origin of the Huize carbonate-hosted Zn-Pb-(Ag) District, Yunnan, South China. Ore Geol. Rev. 31, 360–383.
Han, Y.S., Seong, H.J., Chon, C.M., 2017. Interaction of Sb(III) with iron sulfide under anoxic conditions similarities and differences compared to As(III) interactions. Chemosphere 195, 762–770.
He, B., Xu, Y.G., Huang, X.L., Luo, Z.Y., Shi, Y.R., Yang, Q.J., Yu, S.Y., 2007. Age and duration of the Emeishan flood volcanism, SW China: geochemistry and SHRIMP zircon U-Pb dating of silicic ignimbrites, post-volcanic Xuanwei Formation and clay tuff at the Chaotian section. Earth Planet. Sci. Lett. 255 (3–4), 306–323.
Höll, R., Kling, M., Schroll, E., 2007. Metallogenesis of germanium—a review. Ore Geol. Rev. 30 (3–4), 145–180.
Hu, R.Z., Fu, S.L., Huang, Y., Zhou, M.F., Fu, S.H., Zhao, C.H., Wang, Y.J., Bi, X.W., Xiao, J., 2017. The giant South China Mesozoic low-temperature metallogenic domain: reviews and a new geodynamic model. J. Asian Earth Sci. 137, 9–34.
Hu, Y.S., Ye, L., Huang, Z.L., Wei, C., Danyushevsky, L., 2019. Distribution and existing forms of trace elements from Maliping Pb-Zn deposit in Northeastern Yunnan, China: A LA-ICPMS study. Acta Petrol. Sin. https://doi.org/10.18654/1000-0569/2019.11.00. (in Chinese with English abstract).
Hu, Y.S., Ye, L., Li, Z.L., Huang, Z.L., Zhang, J.W., 2018. Genesis of fahlore in the Tianbaoshan lead–zinc deposit, Sichuan Province, China: a scanning electron microscopy–energy dispersive spectroscopy study. Acta Geochim. 37 (6), 842–853.
Hu, Z., Gao, S., 2008. Upper crustal abundances of trace elements: a revision and update. Chem. Geol. 253 (3–4), 205–221.
Huang, D.H., 2003. Mineralogical character of hemimorphite from the oxidized zone of the Lehong Pb-Zn deposit in Yunnan Province and its significance. Acta Petrol. Mineral. 31 (4), 349–354 (in Chinese with English abstract).
Huang, Z.L., Chen, J., Han, R.S., Li, W.B., Liu, C.Q., Zhang, Z.L., Ma, D.Y., Gao, D.R., Yang, H.L., 2004. In: Geochemistry and Ore-formation of the Huize Giant Lead-zinc Deposit, Yunnan Province, China: Discussion on the Relationship between the Emeishan Flood Basalts and Lead–zinc Mineralization. Geological Publishing House, Beijing, pp. 1–214 (in Chinese).
Jin, Z.G., 2008. In: The Ore-control Factors, Ore-forming Regularity and Ore forecasting of Pb-Zn Deposits in NW Guizhou Province. Engine Industry Press, Beijing, pp. 1–105 (in Chinese with English abstract).
Johan, Z., 1988. Indium and germanium in the structure of sphalerite: an example of coupled substitution with copper. Mineral. Petrol. 39, 211–229.
Johan, Z., Oudin, E., 1986. Présence de grenats, $Ca_3Ga_2(GeO_4)_3$, $Ca_3Al_2((Ge, Si)O_4)_3$ et d'un équivalent ferrifère, germanifère et gallifère de la sapphirine, $Fe_4(Ga, Sn, Fe)_4(Ga, Ge)_6O_{20}$, dans la blende des gisements de la zone axiale pyrénéenne. Conditions de la formation des phases germanifères et gallifères. Comptes Rendus de l'Académie des Sciences Series IIA (Earth Planet. Sci.) 303, 811–816.
Johan, Z., Oudin, E., Picot, P., 1983. Analogues germanifères et gallifères des silicates et oxydes dans les gisements de zinc des Pyrénées centrales, France: argutite et carboirite, deux nouvelles espèces minerales. Tschermaks Mineralogisch – Petrographische Mitteilungen 31, 97–119.
Kelley, K.D., Leach, D.L., Johnson, C.A., Clark, J.L., Fayek, M., Slack, J.F., Anderson, V.M., Ayuso, R.A., Ridley, W.I., 2004. Textural, compositional, and sulfur isotope variations of sulfide minerals in the Red Dog Zn-Pb-Ag deposits, Brooks Range, Alaska: implications for ore formation. Econ. Geol. 99, 1509–1532.
Li, H.K., Zhang, C.L., Yao, C.Y., Xiang, Z.Q., 2013. U-Pb zircon age and Hf isotope compositions of Mesoproterozoic sedimentary strata on the western margin of the Yangtze massif. Sci. China Earth Sci. 56 (4), 628–639.
Li, W.B., Huang, Z.L., Wang, Y.X., Chen, J., Han, R.S., Xu, C., Guan, T., Yin, M.D., 2004. Age of the giant Huize Pb-Zn deposits determined by Sm-Nd dating of hydrothermal calcite. Geol. Rev. 50, 189–195 (in Chinese with English abstract).
Li, X.J., Wu, M.D., Duan, J.S., 1984. The stratigraphic seqence of the Kunyang Group and its top and bottom boundaries. Geol. Rev. 30 (5), 399–408 (in Chinese with English abstract).
Lin, Z.Y., Wang, D.H., Zhang, C.Q., 2010. Rb–Sr isotopic age of sphalerite from the Paoma lead–zinc deposit in Sichuan Province and its implications. Chin. Geol. 37, 488–494 (in Chinese with English abstract).
Liu, H.C., Lin, W.D., 1999. Study on the Law of Pb-Zn-Ag Ore Deposit in Northeast Yunnan. Yunnan University Press, Kunming, China 1–468 (in Chinese).
Möller, P., 1987. Correlation of homogenization temperatures of accessory minerals from sphalerite-bearing deposits and Ga/Ge model temperatures. Chem. Geol. 61, 153–159.
Möller, P., Dulski, P., 1996. Germanium and gallium distribution in sphalerite: a key to the genesis of sediment-hosted sulphide mineralizations. Z. Geol. Wiss. 24 (3–4), 527–538.
Morales-Ruano, S., Touray, J.C., Barbanson, L., Hach-Ali, P.F., 1996. Primary cavities with incompatible fluid fillings in Ge-bearing sphalerite from Cerro del Toro, Alpujarride (Spain). Econ. Geol. 91, 460–465.
Murakami, H., Ishihara, S., 2013. Trace elements of Indium-bearing sphalerite from tin-polymetallic deposits in Bolivia, China and Japan: a femto-second LA-ICPMS study. Ore Geol. Rev. 53, 223–243.
Oftedahl, I., 1940. Untersuchungen über die Nebenbestandteile von Erzmineralien norwegischer zinkblendführender Vorkommen. Skrift. Norsk Vidensk. Akad. Oslo, Math. Naturv. Kl. 8, 1–103.
Olsen, N.J., 2016. The Geochemistry of Antimony in Hydrothermal Solutions Victoria University of Wellington Available at: http://researcharchive.vuw.ac.nz/handle/10063/5557.
Paton, C., Hellstrom, J., Paul, B., Woodhead, J., Hergt, J., 2011. Iolite: freeware for the visualisation and processing of mass spectrometric data. J. Anal. At. Spectrom. 26 (12), 2508–2518.
Pokrovski, G.S., Schott, J., 1998. Thermodynamic properties of aqueous Ge(IV) hydroxide complexes from 25 to 350 °C: implications for the behaviour of germanium and the Ge/Si ratio in hydrothermal fluids. Geochim. Cosmochim. Acta 62, 1631–1642.
Reid, A., Wilson, C.J.L., Shun, L., Person, N., Belousova, E., 2007. Mesozoic plutons of the Yidun Arc, SW China: U/Pb geochronology and Hf isotopic signature. Ore Geol. Rev. 31 (1–4), 88–106.
Renock, D., Becker, U., 2011. A first principles study of coupled substitution in galena. Ore Geol. Rev. 42, 71–83.
Rosenberg, E., 2009. Germanium: environmental occurrence, importance and speciation. Rev. Environ. Sci. Bio/technol. 8 (1), 29–57.
Sharp, T.G., Buseck, P.R., 1993. The distribution of Ag and Sb in galena; inclusions versus solid solution. Am. Mineral. 78, 85–95.
Shannon, R., 1976. Revised effective ionic radii and systematic studies of interatomic distances in halides and chalcogenides. Acta crystallogr. A, Found. Crystallogr. 32, 751–767.
Sun, Z.M., et al., 2009. SHRIMP U-Pb dating and its stratigraphic significance of tuff zircons from Heishan Formation of Kunyang Group, Dongchuan area, Yunnan Province, China. Geol. Bull. China 28 (7), 896–900 (in Chinese with English abstract).
Thomas, D.W., Mahmood, T., Lindhal, C.B., 2000. Germanium and germanium compounds. Kirk-Othmer Encyclopedia of Chemical Technology. John Wiley and Sons Inc.
Wang, X.C., 1992. Genesis analysis of the Tianbaoshan Pb-Zn deposit. J. Chengdu College Geol. 19 (3), 10–20 (in Chinese with English abstract).
Warren, H.V., Thompson, R.M., 1945. Sphalerites from western Canada. Econ. Geol. 40, 309–335.
Wei, C., Huang, Z.L., Yan, Z.F., Hu, Y.S., Ye, L., 2018a. Trace element contents in sphalerite from the Nayongzhi Zn-Pb Deposit, Northwestern Guizhou, China: insights into incorporation mechanisms, metallogenic temperature and ore genesis. Minerals 8 (11), 490. https://doi.org/10.3390/min8110490.
Wei, C., Ye, L., Huang, Z.L., Gao, W., Hu, Y.S., Li, Z.L., Zhang, Z.W., 2018b. Ore genesis and geodynamic setting of Laochang Ag-Pb-Zn-Cu deposit, Southern Sanjiang Tethys Metallogenic Belt, China: constraints from whole rock geochemistry, trace elements in sphalerite, Zircon U-Pb Dating and Pb Isotopes. Minerals 8 (11), 516. https://doi.org/10.3390/min8110516.
Wernick, J.H., 1960. Constitution of the $AgSbS_2$-PbS, $AgBiS_2$-PbS, and $AgBiS_2$-$AgBiSe_2$ systems. Am. Mineral. 45, 591–598.
Wu, Y., 2013. The age and ore-forming process of MVT deposits in the boundary area of Sichuan-Yunnan-Guizhou provinces, Southwest China PhD thesis. China University of Geosciences, Beijing, 1-167 (in Chinese with English abstract).
Yan, D.P., Zhou, M.F., Song, H.L., Wang, X.W., Malpas, J., 2003. Origin and tectonic significance of a Mesozoic multi-layer over-thrust system within the Yangtze Block (South China). Tectonophysics 361, 239–254.
Ye, L., Cook, N.J., Ciobanu, C.L., Liu, Y.P., Zhang, Q., Liu, T.G., Gao, W., Yang, Y.L., Danyushevskiy, L., 2011. Trace and minor elements in sphalerite from base metal deposits in South China: a LA-ICPMS study. Ore Geol. Rev. 39 (4), 188–217.
Ye, L., Li, Z.L., Hu, Y.S., Huang, Z.L., Zhou, Z.J., Fan, H.F., Danyushevskiy, L., 2016. Trace element in sulfide from Tianbaoshan Pb-Zn deposit, Sichuan province, China: a LA-ICPMS study. Acta Petrol. Sin. 32 (11), 3377–3393 (in Chinese with English abstarct).
Yuan, B., Zhang, C.Q., Yu, H.J., Yang, Y.M., Zhao, Y.X., Zhu, C.C., Ding, Q.F., Zhou, Y.B., Yang, J.C., Xu, Y., 2017. Element enrichment characteristics: insights from element geochemistry of sphalerite in Daliangzi Pb-Zn deposit, Sichuan, Southwest China. J. Geochem. Explor. 186, 187–201.
Zhang, C.Q., Wu, Y., Hou, L., Mao, J.W., 2015. Geodynamic setting of mineralization of Mississippi Valley-type deposits in world-class Sichuan-Yunnan-Guizhou Zn-Pb triangle, southwest China: implications from age-dating studies in the past decade and the Sm-Nd age of Jinshachang deposit. J. Asian Earth Sci. 103, 103–114.
Zhang, Q., 1987. Trace elements in galena and sphalerite and their geochemical significance in distinguishing the genetic types of Pb-Zn ore deposits. Chin. J. Geochem. 6, 177–190.
Zhang, Y.X., Wu, Y., Tian, G., Shen, L., Zhou, Y.M., Dong, W.W., Zeng, R., Yang, X.C., Zhang, C.Q., 2014. Mineralization Age and the Source of Ore-forming Material at Lehong Pb-Zn Deposit, Yunnan Province: constraints from Rb-Sr and S Isotopes System. Acta Mineral. Sin. 34 (3), 305–311.
Zhao, D., Han, R.S., Ren, T., Wang, J.S., Wu, H.Z., Zhang, X.P., Cui, J.H., 2018. Characteristics of fluid inclusions geochemistry of Lehong large-sized Pb-Zn ore deposit, northeastern Yunnan Province. Mineral Depos. 37 (5), 1018–1036 (in Chinese with English abstract).
Zhou, M.F., Yan, D.P., Kennedy, A.K., Li, Y.Q., Ding, J., 2002. SHRIMP zircon geochronological and geochemical evidence for Neo-Proterozoic arc-related magmatism along the western margin of the Yangtze Block, South China. Earth Planet. Sci. Lett. 196, 1–67.
Zhou, Y.M., 2003. Geological characterisitics of the Lehong Lead-Zinc deposit in Northeastern Yunnan and Its ore-search prospects. Geol. Geochem. 31 (4), 16–21 (in Chinese with English abstract).